Astrophysics of gravitational wave sources

Lecture 1: Evolution of single and binary stars to compact objects

Ondřej Pejcha

ÚTF MFF UK

Mergers due to gravitational wave emission

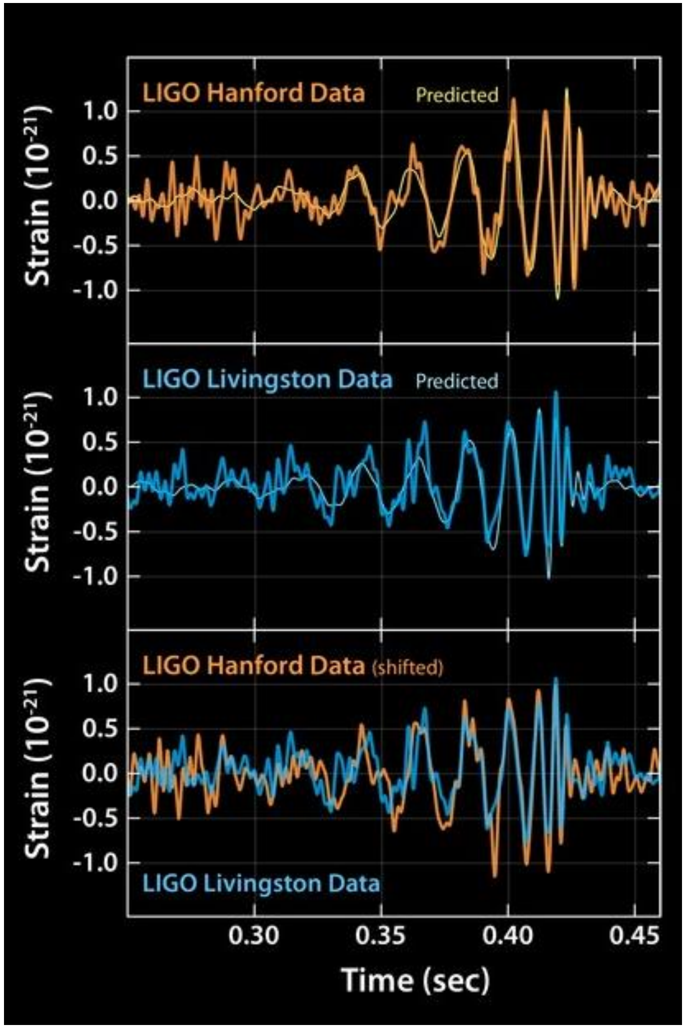

Caltech/MIT/LIGO Lab

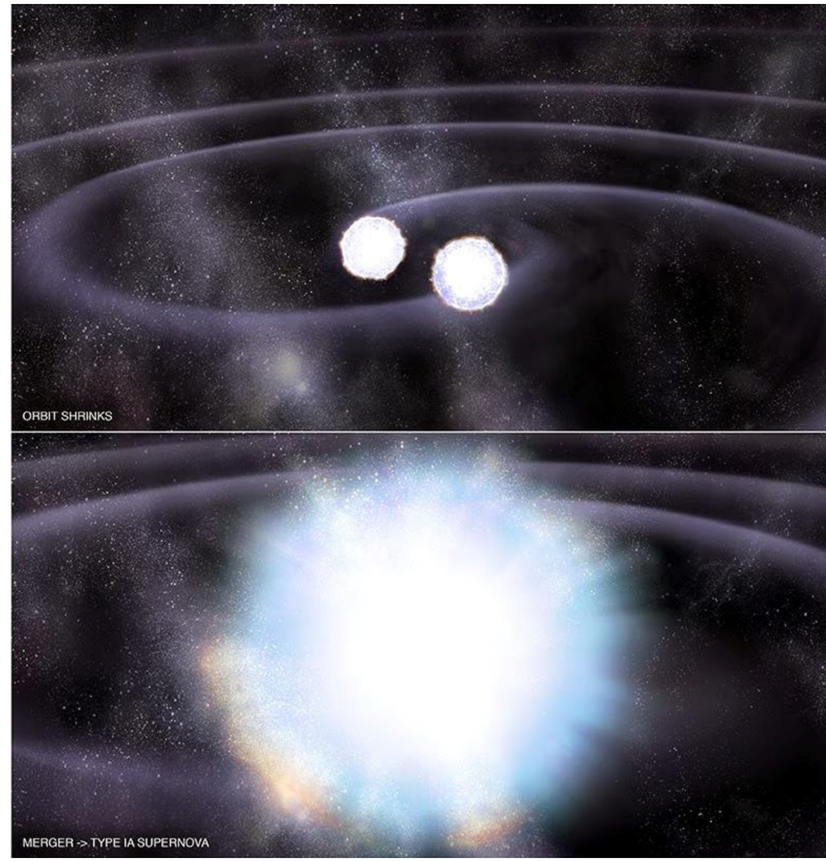

NASA/CXC/M.Weiss

The Origin of the Solar System Elements

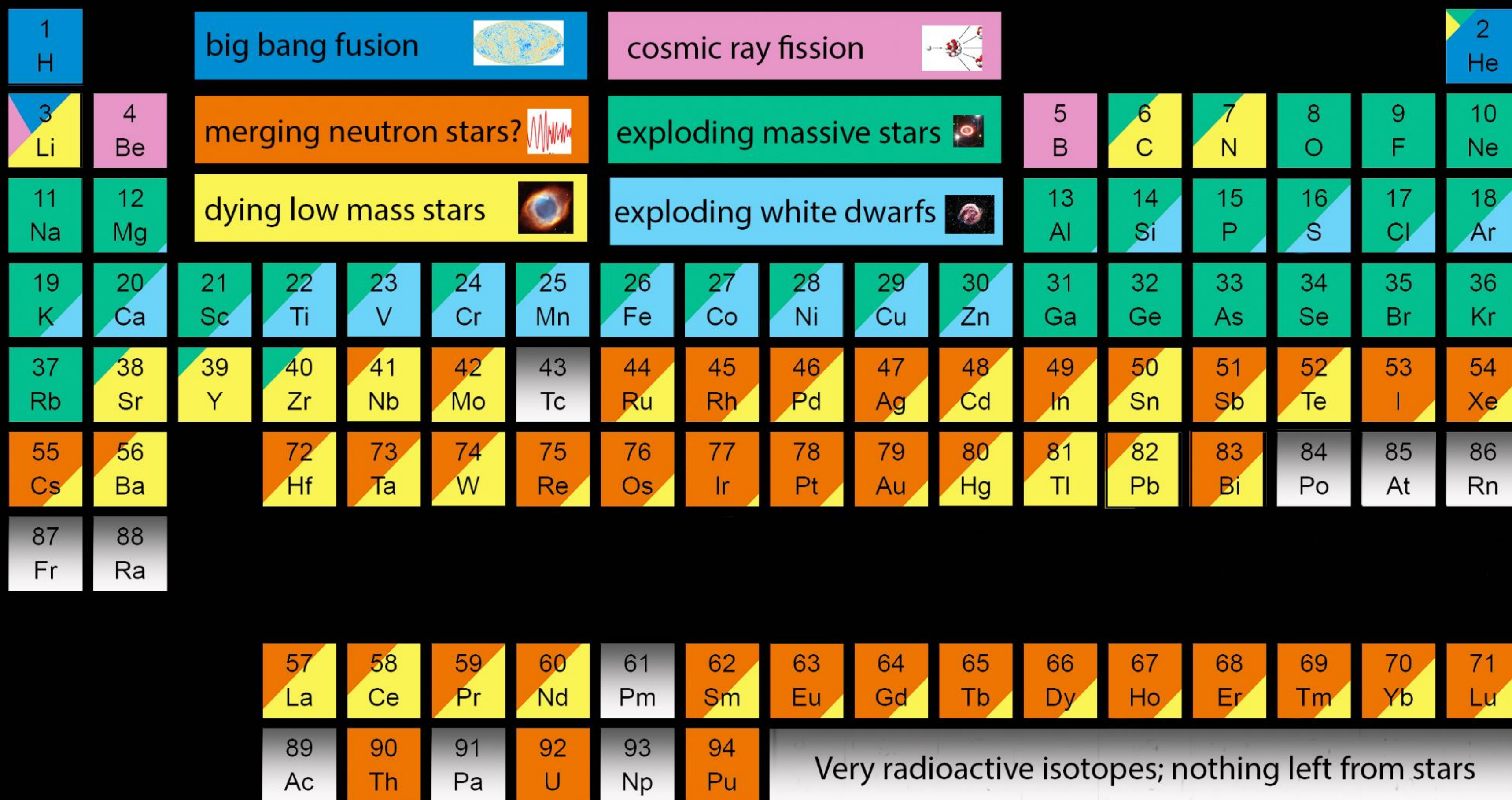

Graphic created by Jennifer Johnson
http://www.astronomy.ohio-state.edu/~jaj/nucleo/

Astronomical Image Credits:
ESA/NASA/AASNova

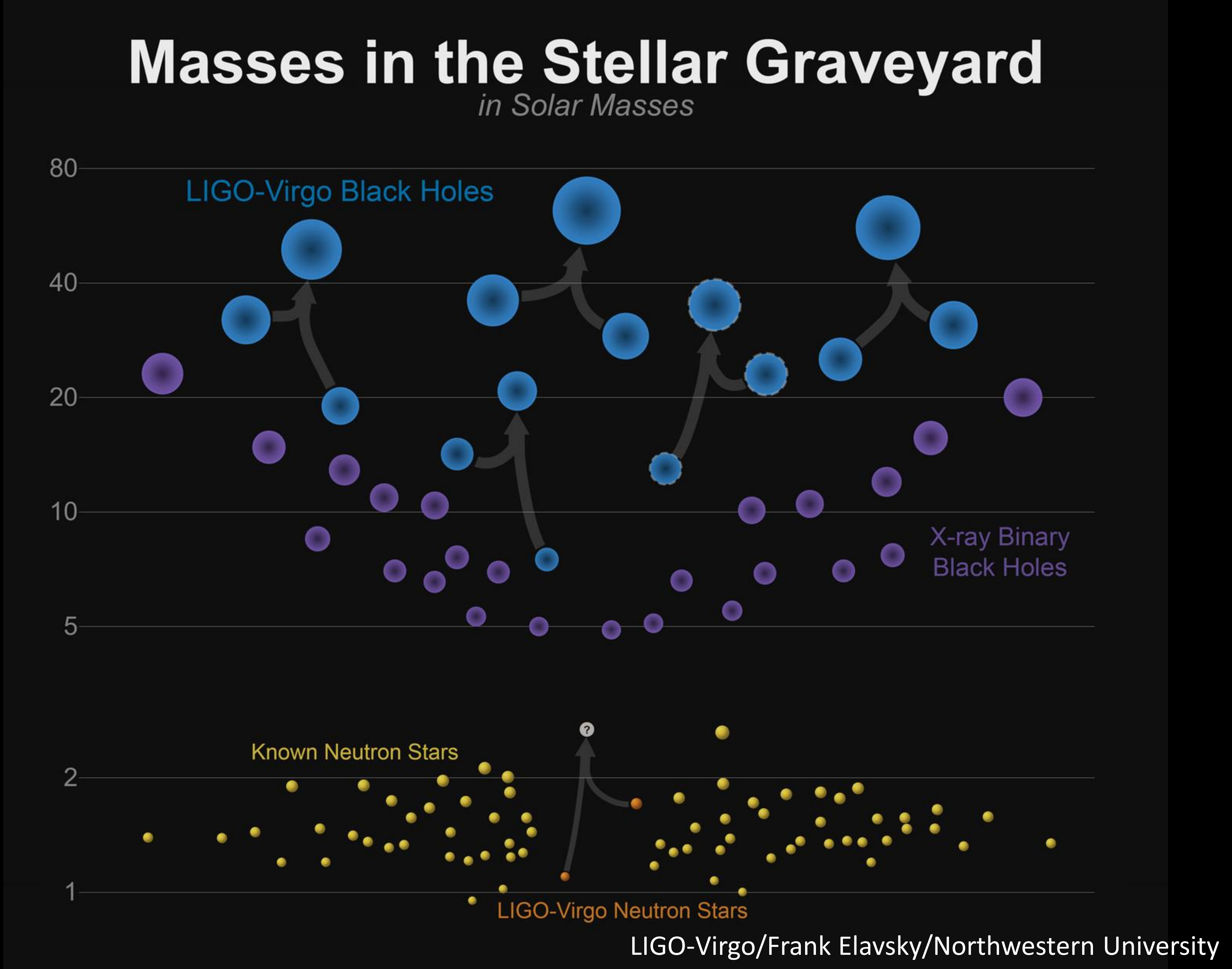
Masses in the Stellar Graveyard
in Solar Masses
80
40
20
10
5
2
1
LIGO-Virgo Black Holes
X-ray Binary
Black Holes
Known Neutron Stars
LIGO-Virgo Neutron Stars
?
LIGO-Virgo/Frank Elavsky/Northwestern University

Single star evolution before core-collapse

Central temperature and pressure

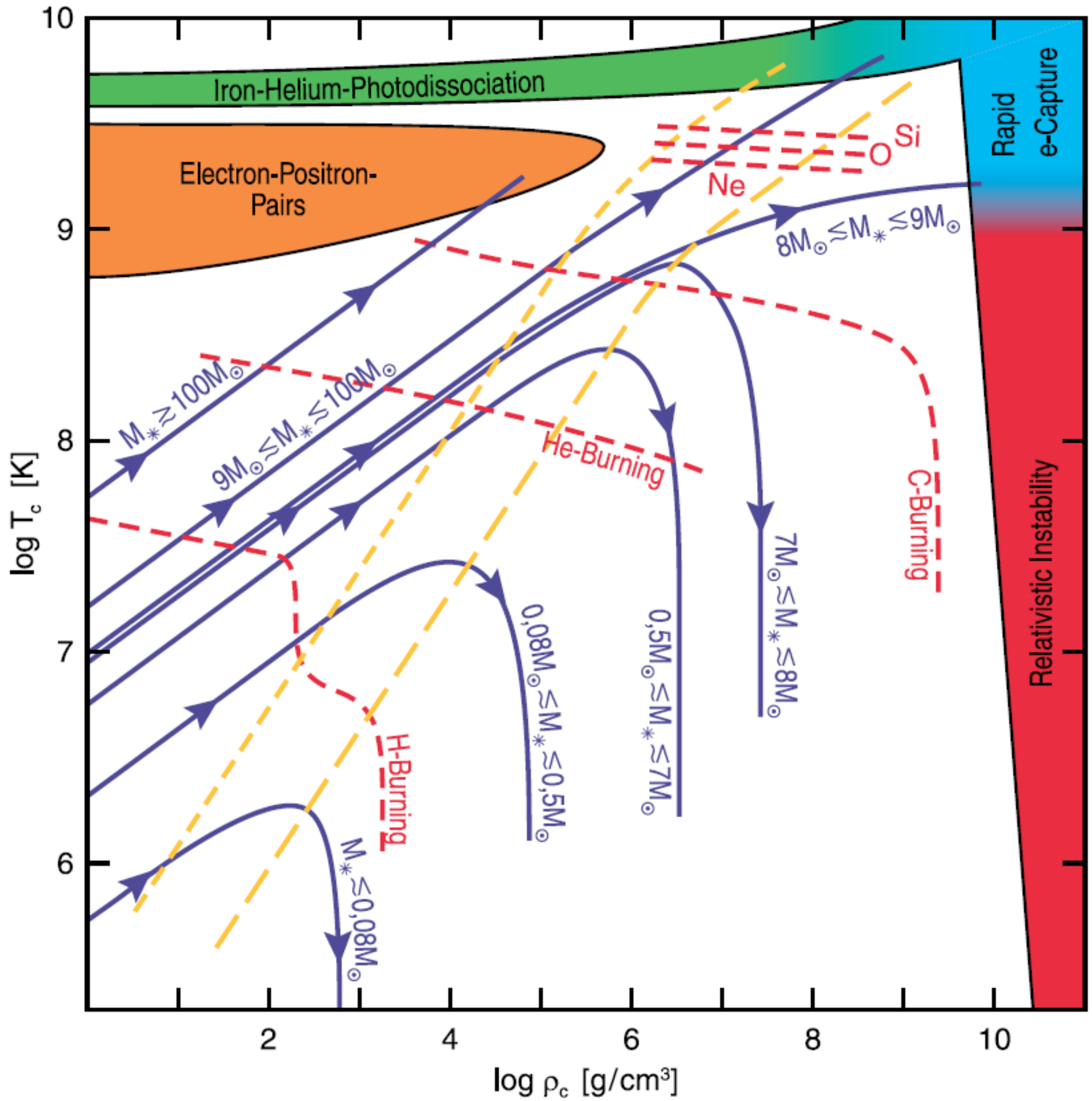

Janka (2012)

Single star evolution before core-collapse

Central temperature and pressure

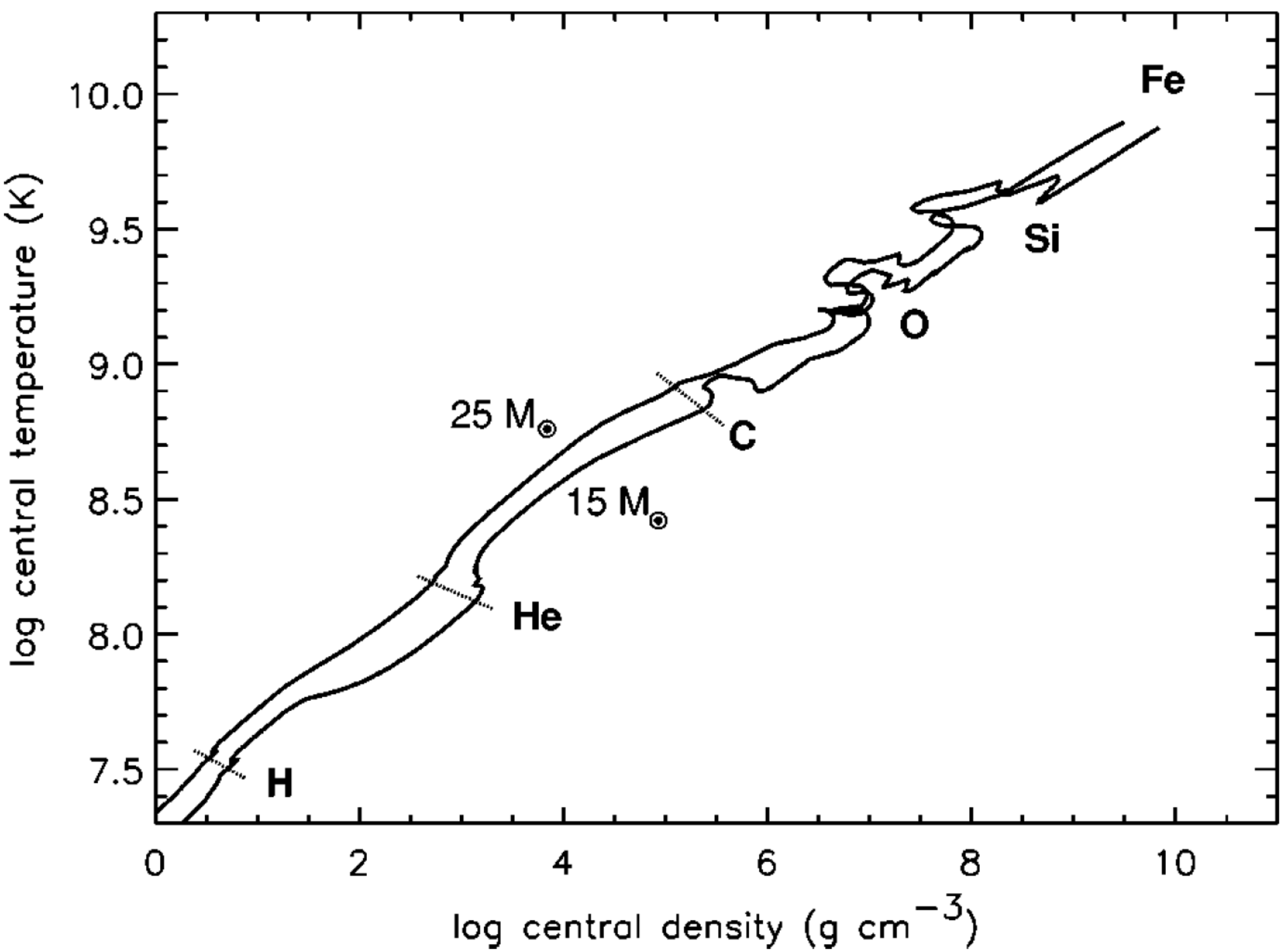

Woosley et al. (2002)

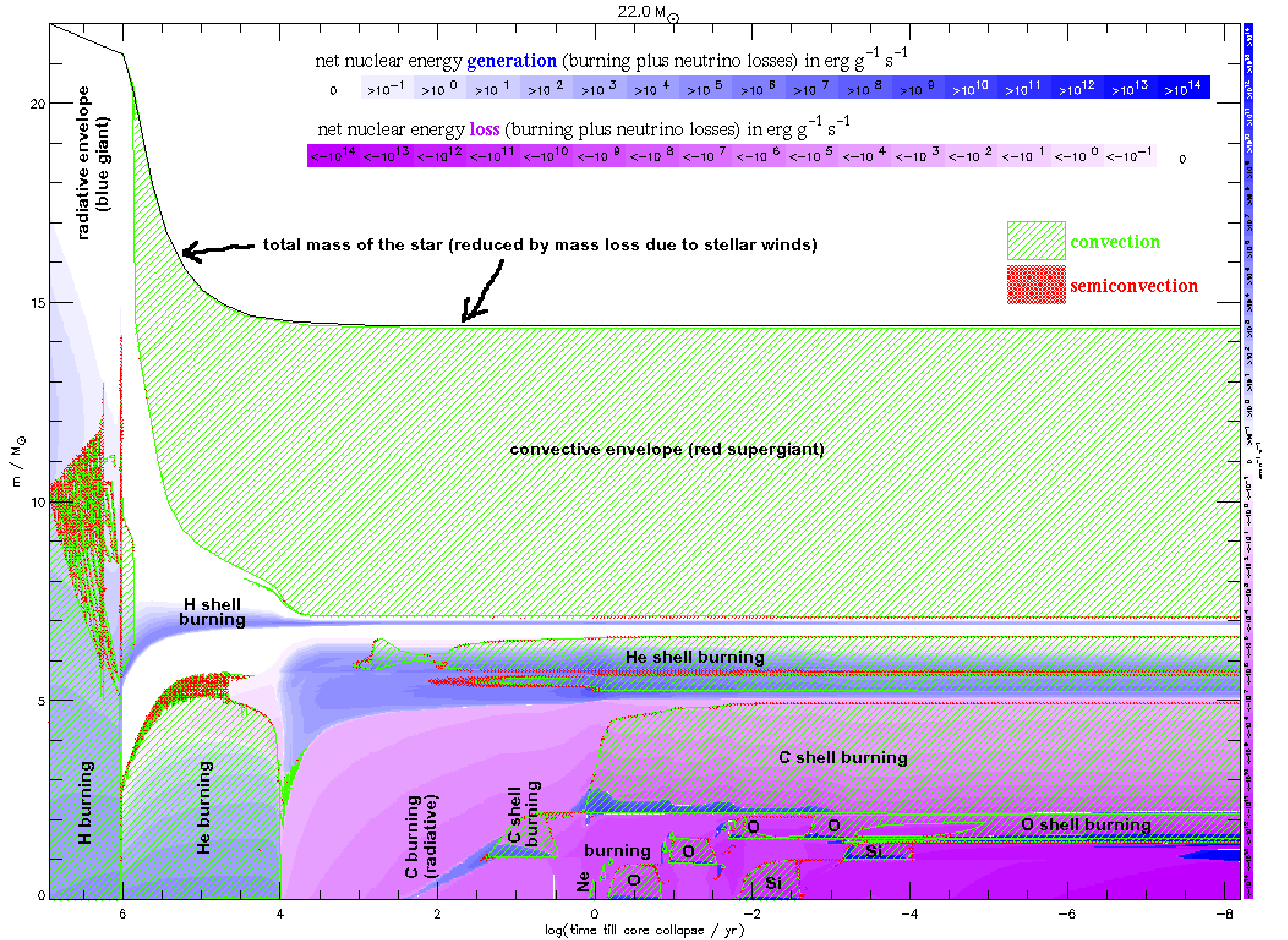

A. Heger website 2sn.org

Physical processes inside massive star

- Neutrino losses
    - Mostly due to thermal processes (T^9), later due to neutronization (T^6)
    - Accelerates evolution (~day timescale for silicon)
- Convection
    - Mixing length theory, but convective and nuclear timescales comparable
    - Mixing as a diffusive process
- Semi-convection
    - Schwarzschild – instability only due to temperature/pressure gradients
    - Ledoux – also takes into account chemical composition
    - Unstable by Schwarzschild & stable by Ledoux = semi-convection
    - Diffusion coefficient uncertain
- Overshoot mixing
    - Modeled by diffusion
- Rotation & magnetic fields
    - Coupling of core to envelope – affected by mass loss
- Mass loss

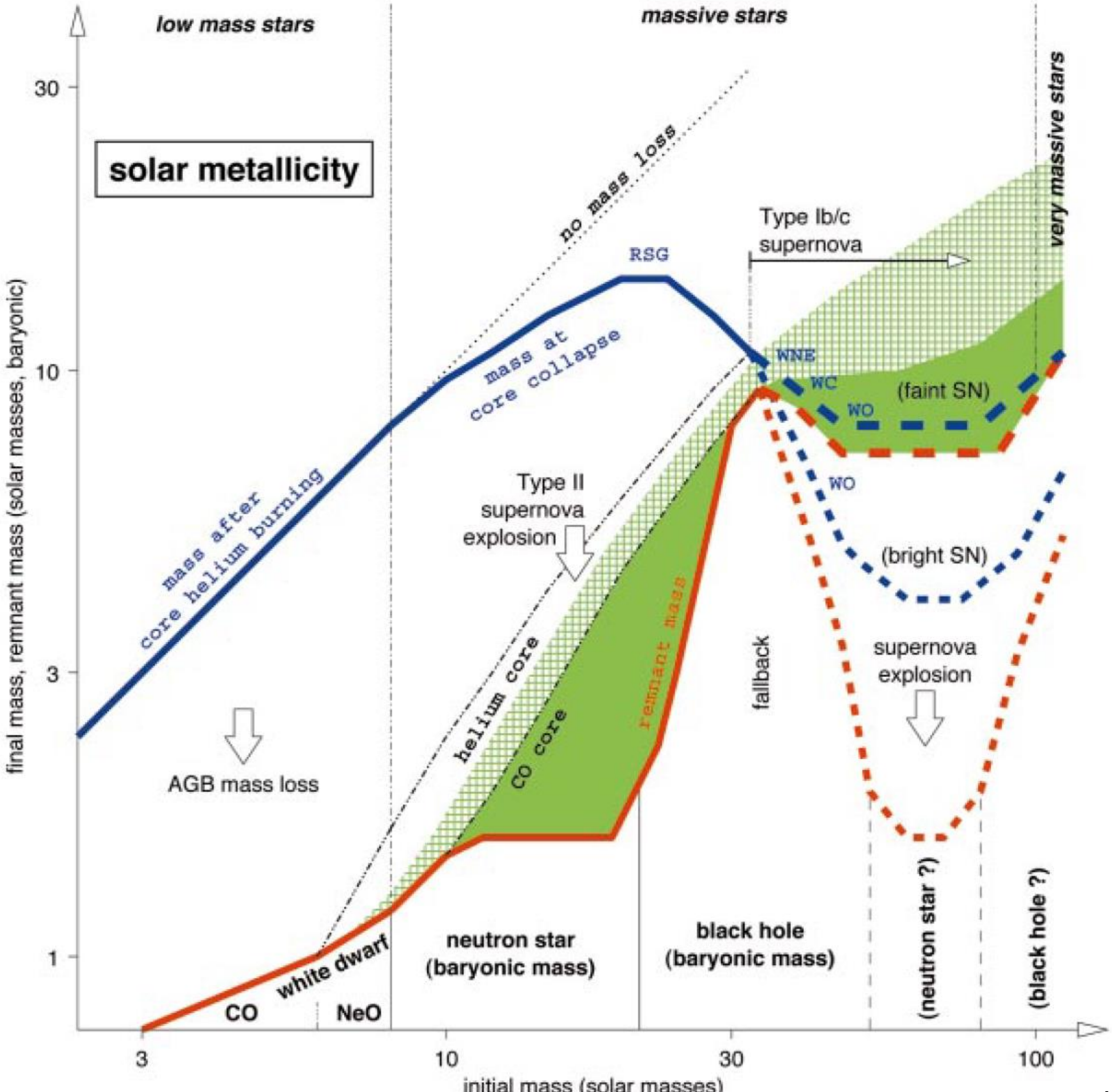

Woosley et al. (2002)

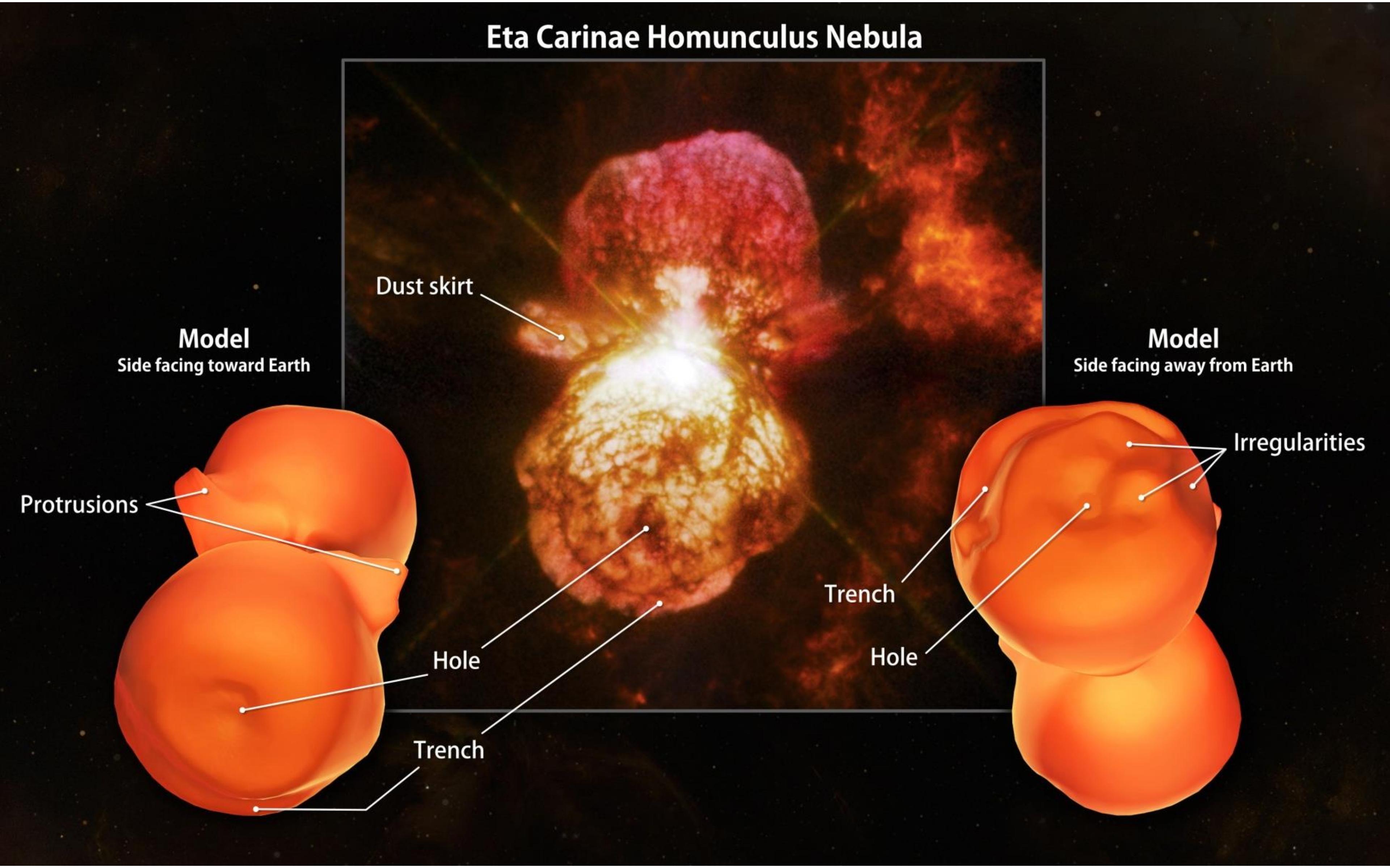

Image Credit: NASA, Goddard Space Flight Center/SVS - Inset: NASA, ESA, Hubble SM4 ERO Team

Chemically-homogeneous evolution

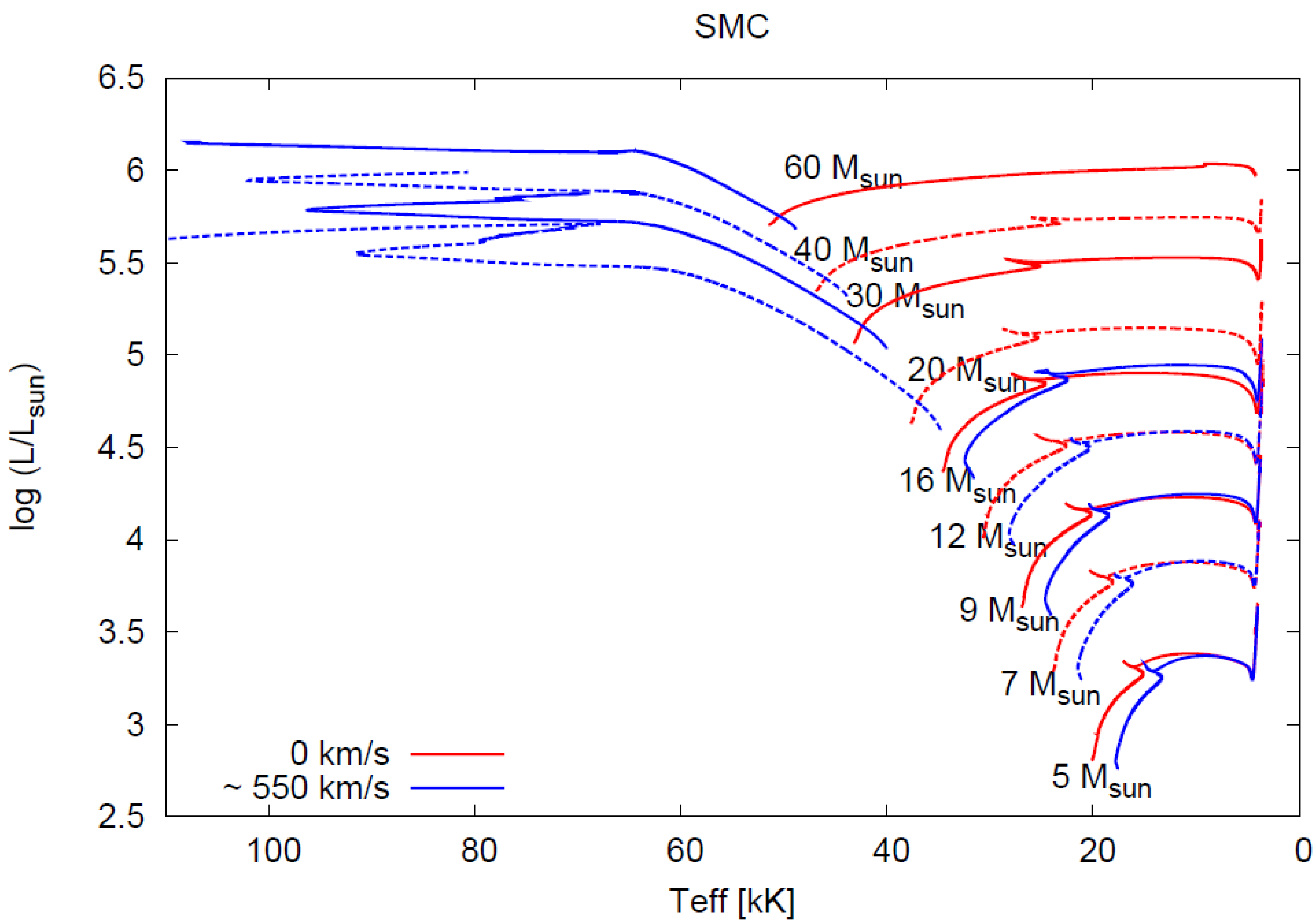

Brotts et al. (2011)

Pair instability

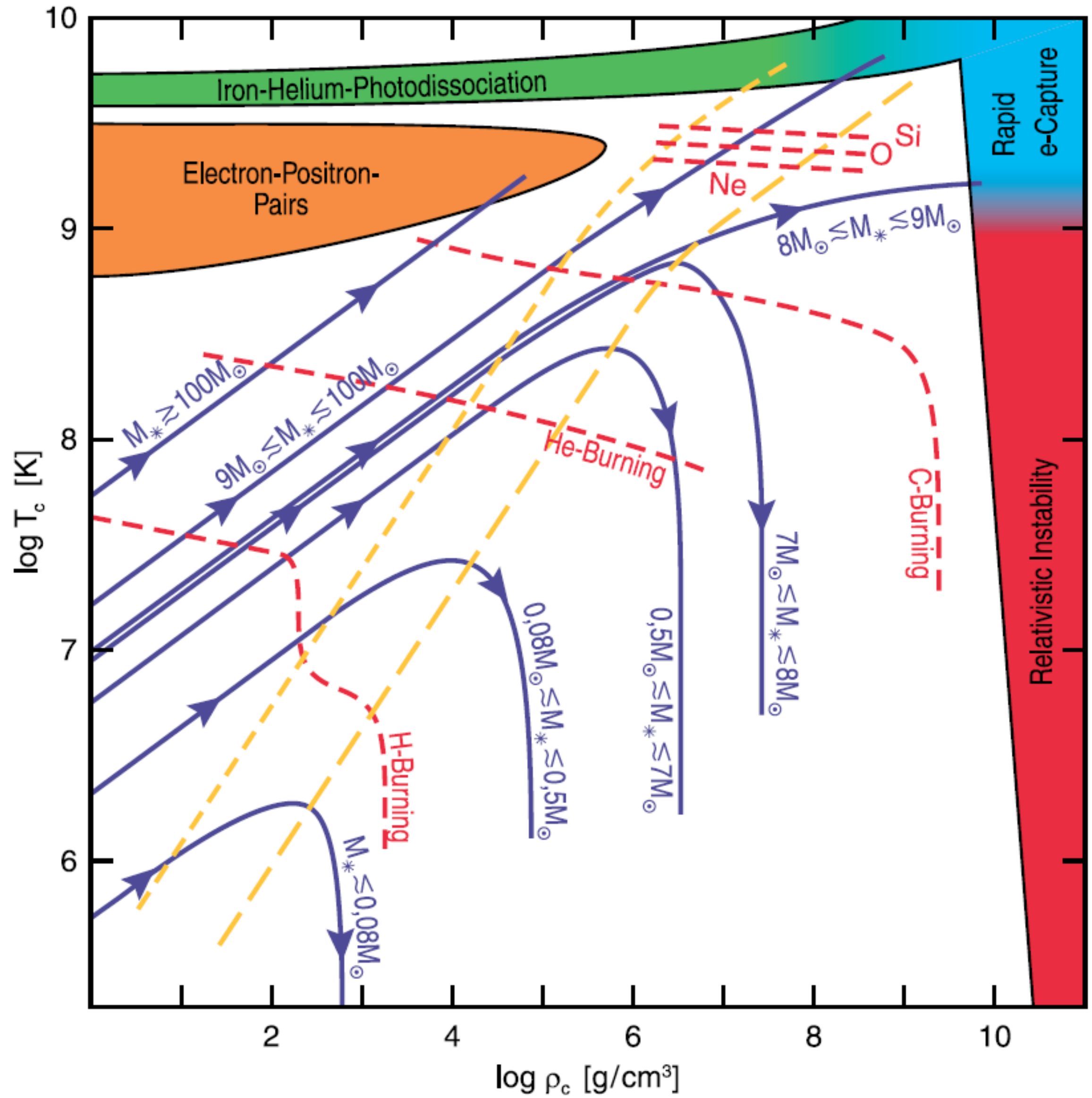

Janka (2012)

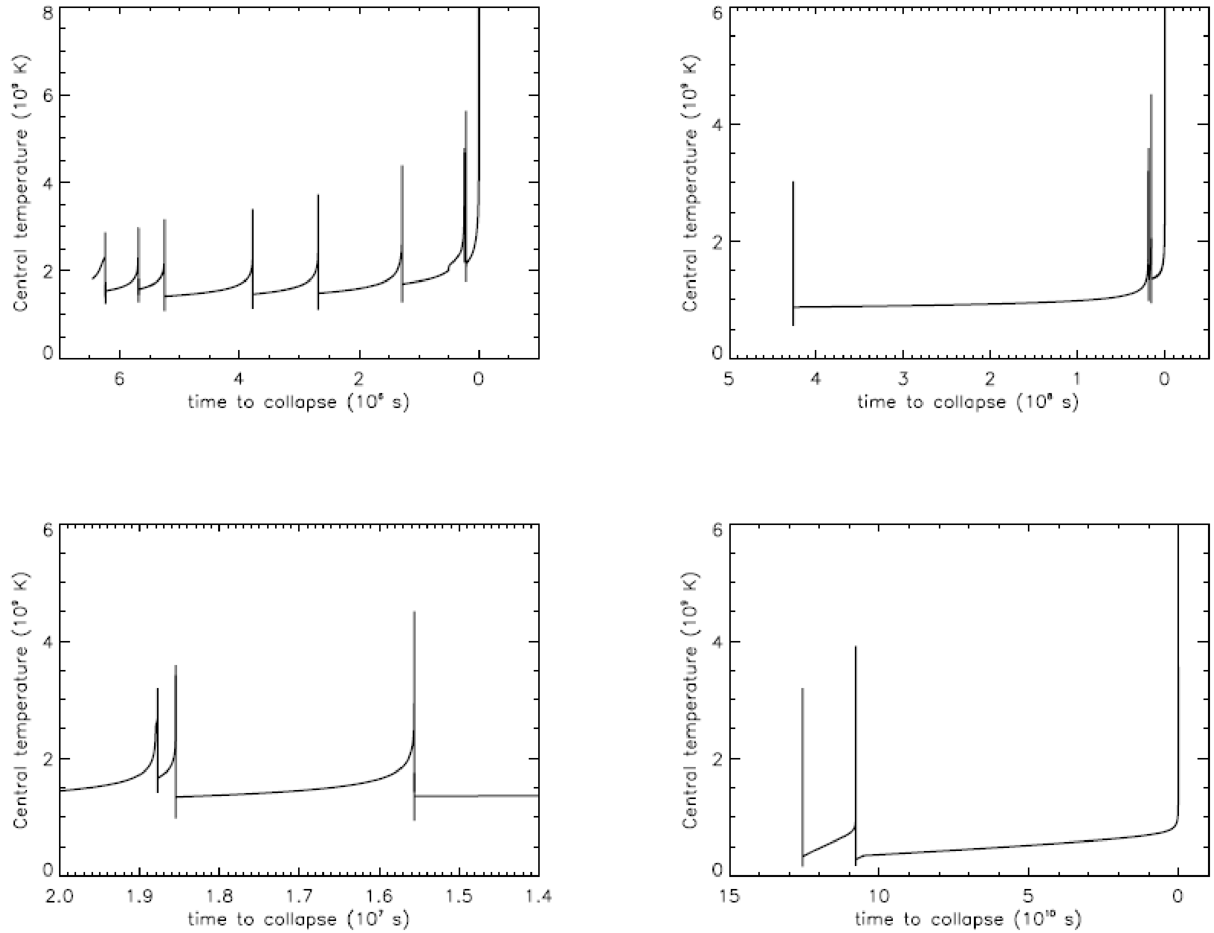

Fig. 2 Pair-driven pulsations cause rapid variations in the central temperature (10^9 K) near the time of death for helium cores of 32, 36, 40, 44, 48, 52 (on two different time scales) and 56 $M_\odot$ (left to right; top to bottom). The log base 10 of the time scales (s) in each panel are respectively 4, 4, 5, 5, 6, 8, 7, and 10. The last rise to high temperature marks the collapse of the iron core to a compact object. More massive cores have fewer, less frequent, but more energetic pulses. All plots begin at central carbon depletion.

Woosley & Heger (2015)

Border between white dwarf and core-collapse

5 Msun

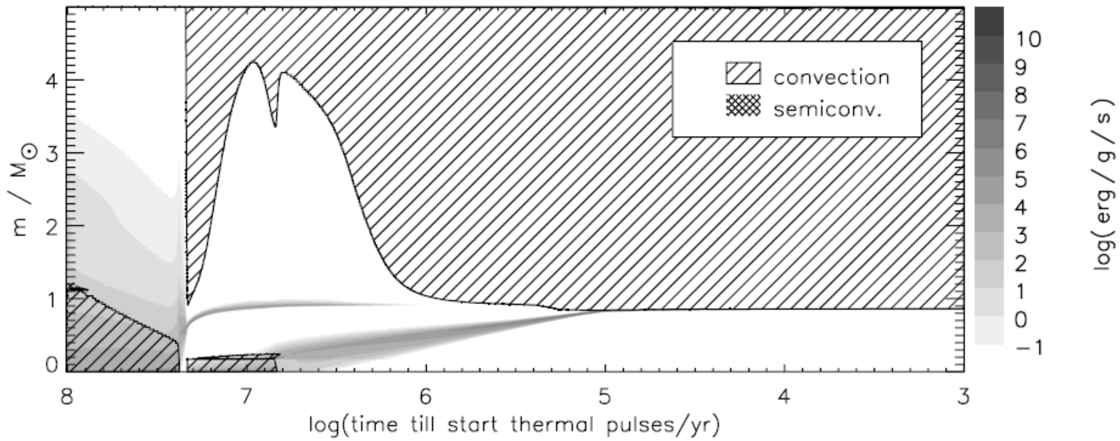

16 Msun

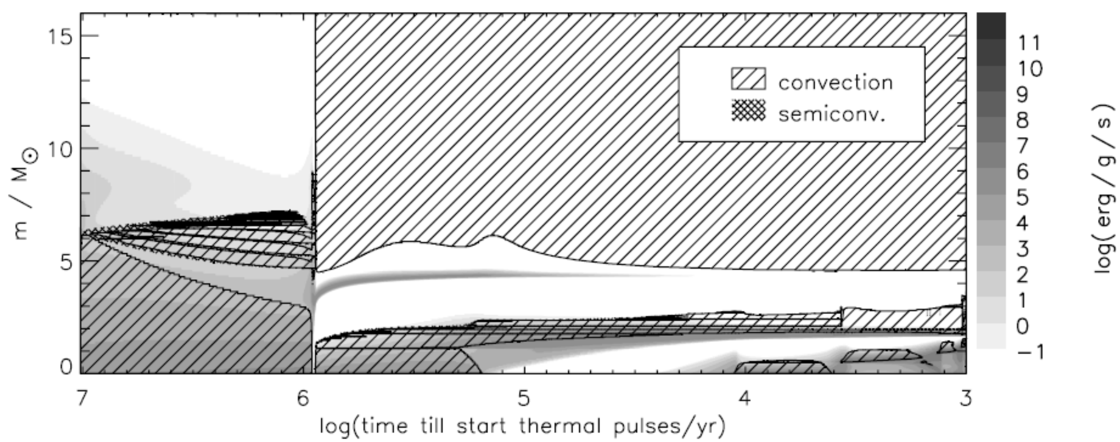

Poelarends et al. (2008)

Empirical evidence

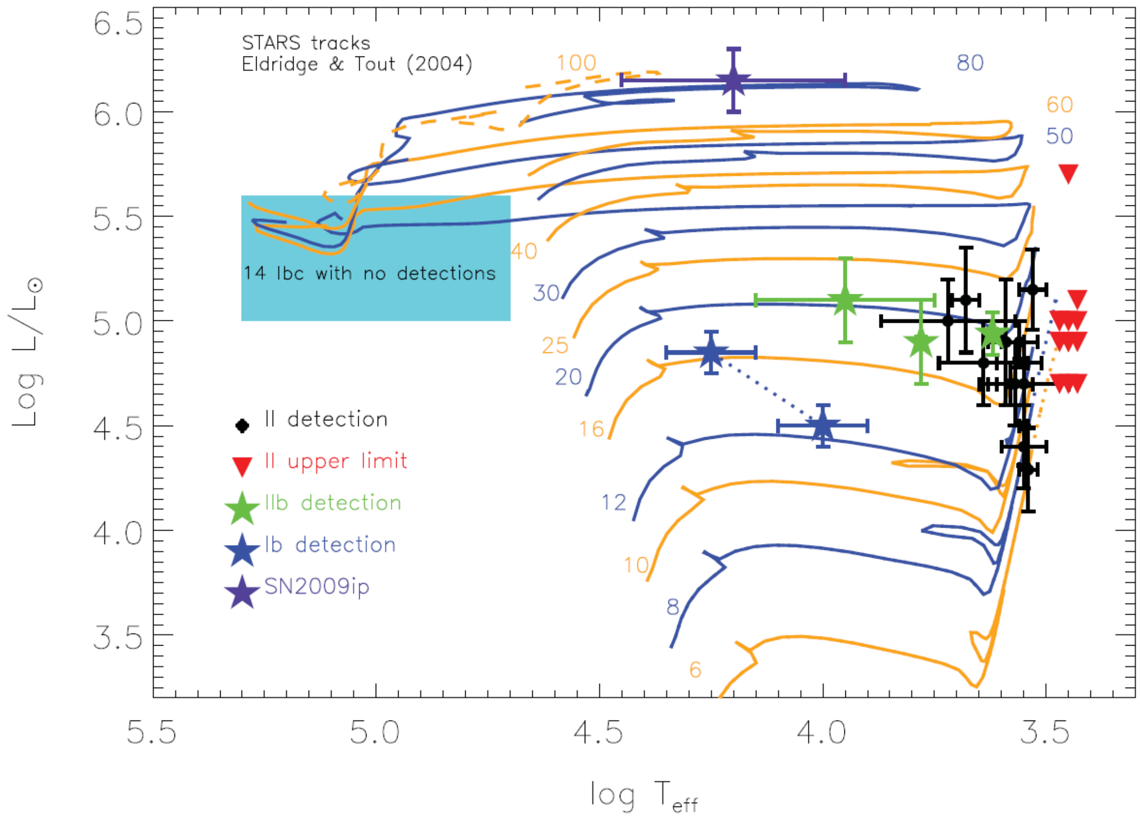

Figure 3. The positions of the detected progenitors and upper limits to the type II SNe as discussed in Section 2. The stellar evolutionary tracks are from Eldridge & Tout (2004). The possible positions of the progenitor star of PTF13bvn is marked with two symbols, joined by the dotted line. These show the two positions of the progenitors proposed by Bersten et al. (2014) and Eldridge et al. (2015) in their binary models. The position of the progenitor of SN2009ip is shown as the magenta symbol, as estimated from the faintest magnitude the LBV star was found at (see Section 2.4 for more details). The 14 Ibc progenitors with no detections are not quantitatively marked here. If they were WR stars, then one would expect to find them around the blue shaded area (although the box position is illustrative as some models predict progenitors outside this locus, e.g. Groh, Georgy, & Ekström 2013a; Groh et al. 2013c) There are 30 progenitors below $\log L = 5.1$, and only one (SN2009ip) above, if indeed SN2009ip is a genuine core-collapse SN.

Smartt (2015)

Red supergiant problem

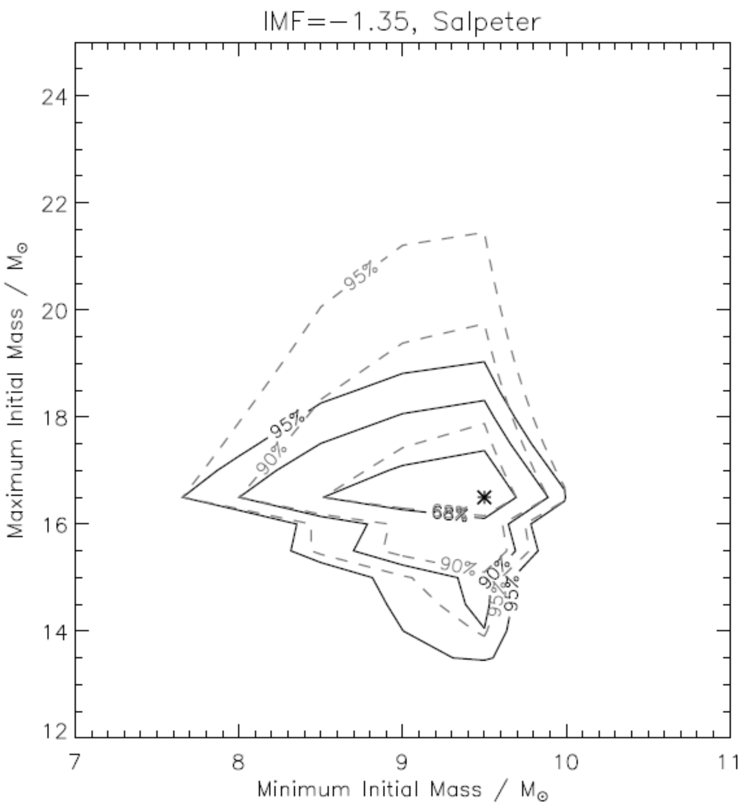

Figure 5. The maximum likelihood of the minimum and maximum initial masses of the type II progenitor distribution, assuming the stars follow a Salpeter IMF. Originally calculated in Smartt et al. (2009), and reproduced here with the updated and extended masses in this review. The dashed lines show the confidence contours (68, 90, and 95%) for the detections only and the solid lines show the confidence contours for the detections and upper limits combined. The star symbol marks the best fit, as described in Section 3.2, of $m_{\rm min} = 9.5^{+0.5}_{-2}$ and $m_{\rm max} = 16.5^{+2.5}_{-2.5}$. This is for the masses from the STARS and Geneva rotating models, the values for the KEPLER masses are given in the text.

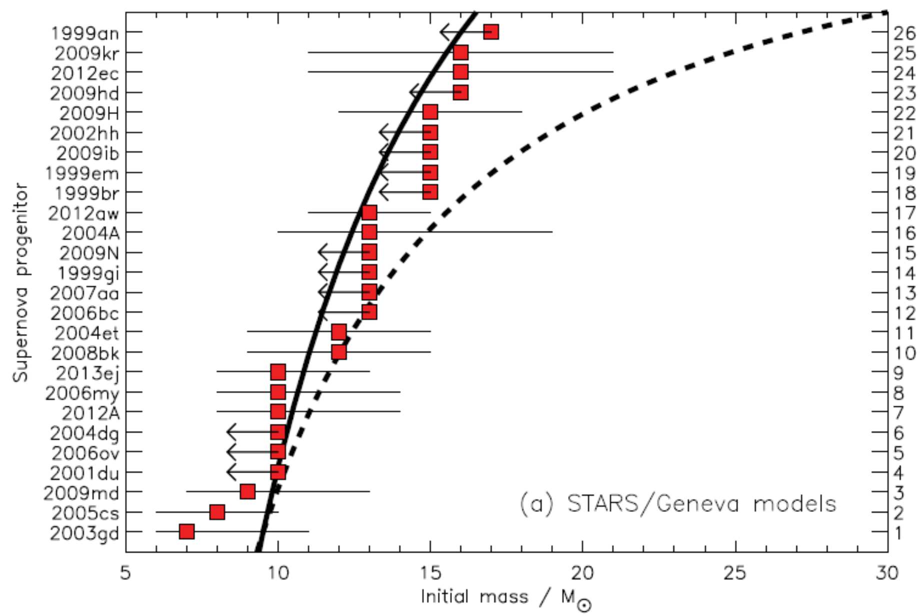

Smartt (2015)

Binary star evolution

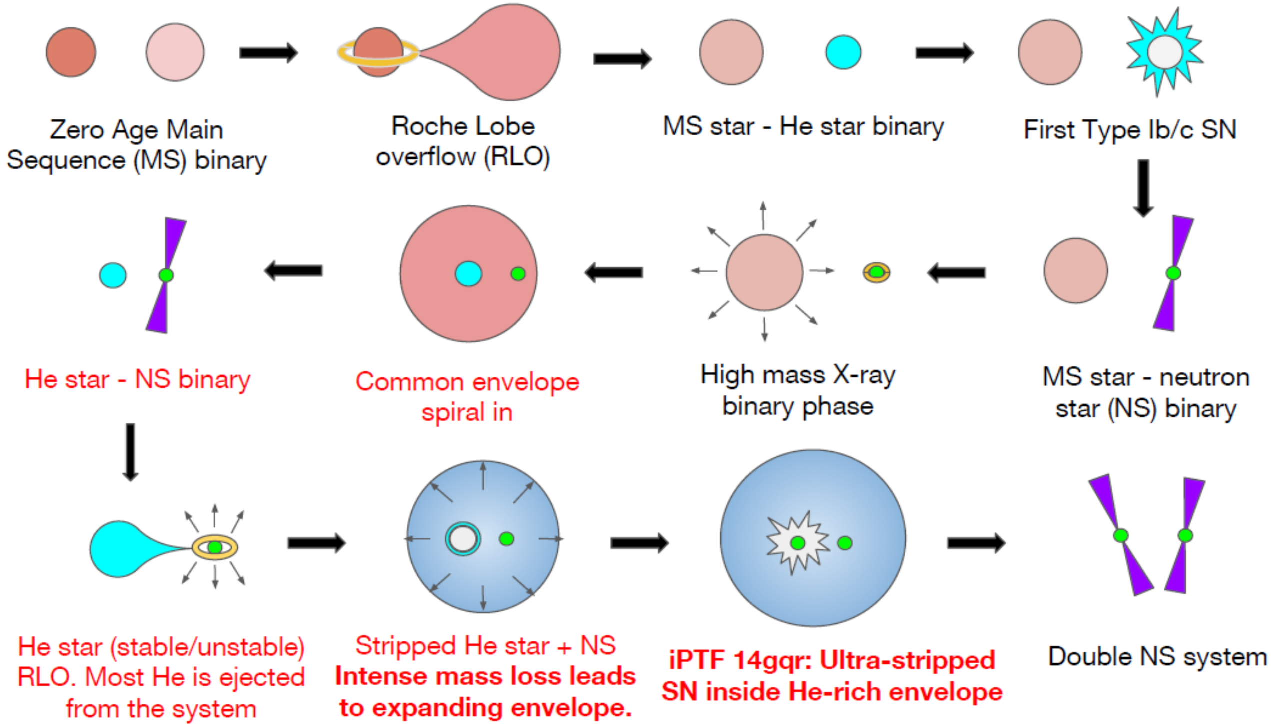

Figure 6: **Stellar evolutionary sequence leading from a binary system of massive stars (starting from the top left) to a NS-NS system, adapted from (*9*).** NS-BH systems are expected to arise from binaries where the first formed compact object is a BH. NS-WD systems follow a similar evolutionary sequence starting from the HMXB stage (where the NS is replaced by the WD), but require additional mass transfer in the earlier stages (*52*). The material composition of the stars is indicated by their colors – red indicates H-rich material, cyan / blue indicate He-rich material, grey indicates CO-rich material and green indicates degenerate matter (in NS). The specific phase of the evolution is indicated by the text next to the systems, with black text indicating phases that have been observed previously, while red text indicates phases that have not been previously observed, and bold red text phases we observed in this work.

De et al. (2018)

Mass transfer

Change in radius of Roche lobe

$$R'_{\mathrm{L}} \equiv \frac{\mathrm{d}\log R_{\mathrm{L}}}{\mathrm{d}\log M_1} = (1+q)\cdot\left(\frac{\mathrm{d}\log R_{\mathrm{L}}/a}{\mathrm{d}\log q} + \frac{\mathrm{d}\log a}{\mathrm{d}\log q}\right),$$
$$\approx 2.13q - 1.67, \quad 0 < q \lesssim 50;$$

Change in radius of star in response to mass loss (stellar structure)

$$R'$$

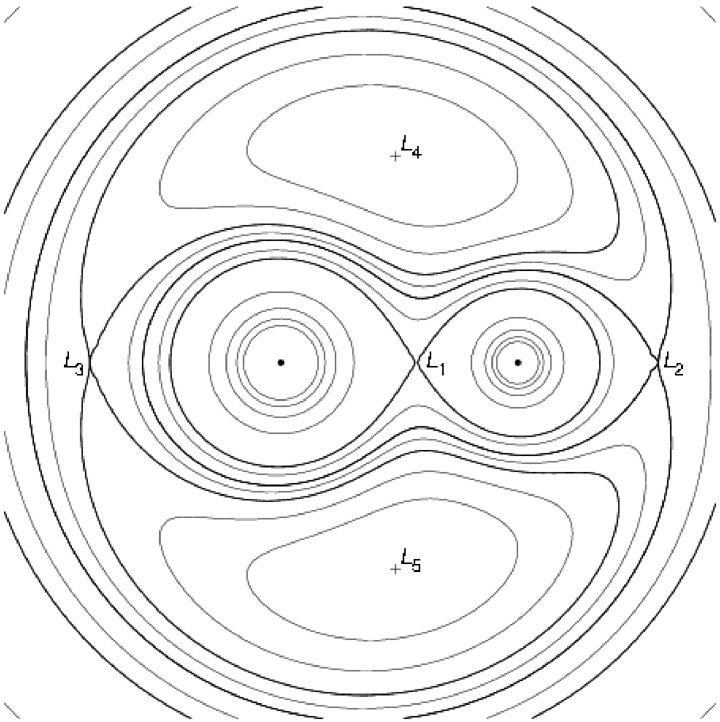

- Nuclear timescale – very slow (main sequence lifetime)
- Thermal timescale (Kelvin-Helmholtz)
- Dynamical timescale

Instability of binary stars

- Dynamically-unstable mass transfer/loss

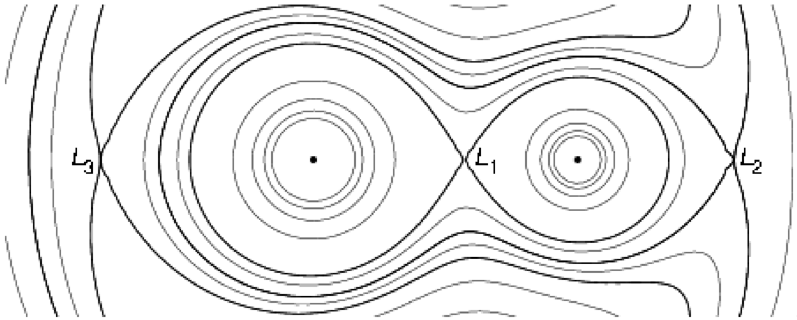

  - adiabatic expansion relative to Roche lobe → instability on dynamical timescale
  - calculation of $\dot{M}(t)$, $R(t)$ complicated by processes near the surface → not entirely adiabatic evolution (Woods & Ivanova 2011; Passy et al. 2012; Pavlovskii & Ivanova 2016)
  - critical mass ratio for red giant between ~0.7 and ~3
- Tidal (Darwin) instability
  - Mass ratio < 0.09 (Rasio 1995)
- Influence of distant companion (Lidov-Kozai)
  - Collisions, Roche lobe overflows
- Difficulties in determining which binaries become unstable translates to uncertainties in evolutionary pathways and rates

Bringing stars in a binary together

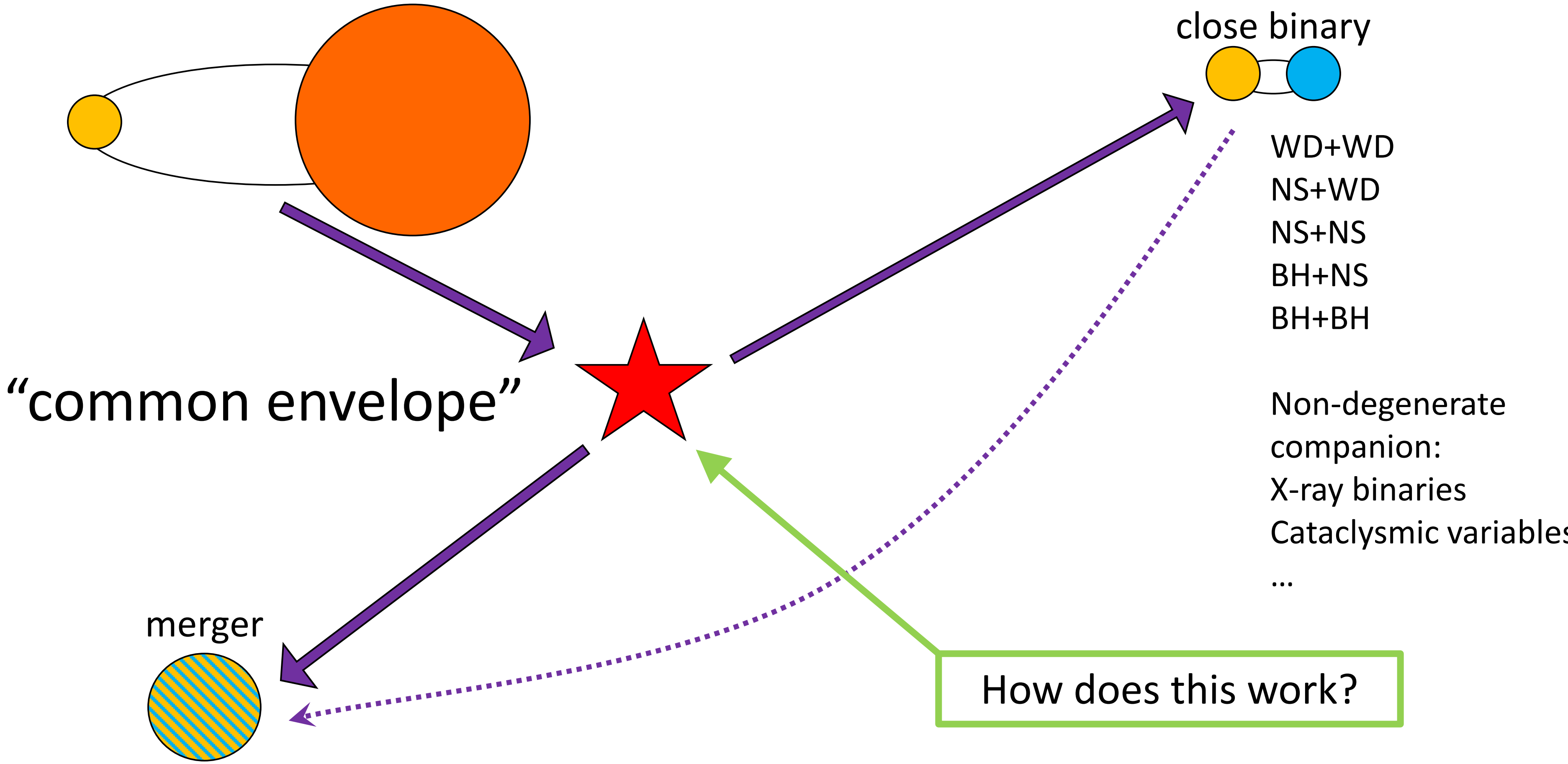

Blue stragglers
SN1987A progenitor
FK Com
η Car
…

SN Ia
short GRB/kilonovae
R CrB
…

Paczynski (1976)
Ostriker (1975)
Iben & Livio (1993)
Taam & Sandquist (2000)
Ivanova et al. (2013)

Common envelope

Dynamical mass transfer so rapid that binary ends up orbiting in non-corotating envelope

$$v = \left(\frac{GM}{A}\right)^{\frac{1}{2}}$$ Orbital velocity

$$D \sim A^2 \ v^2 \ \rho \sim GMA\rho,$$ Drag force

$$L_D \sim Dv \sim D \ \frac{A}{P_{\mathrm{orb}}} \sim \frac{GMA^2}{P_{\mathrm{orb}}} \ \rho,$$ Drag luminosity

$$L_D \sim \frac{d}{\mathrm{d}t} \ \ \frac{GM^2}{A} \ \ \sim \frac{GM^2}{\tau_D A},$$ Effect of drag luminosity on orbit

Paczynski (1976)

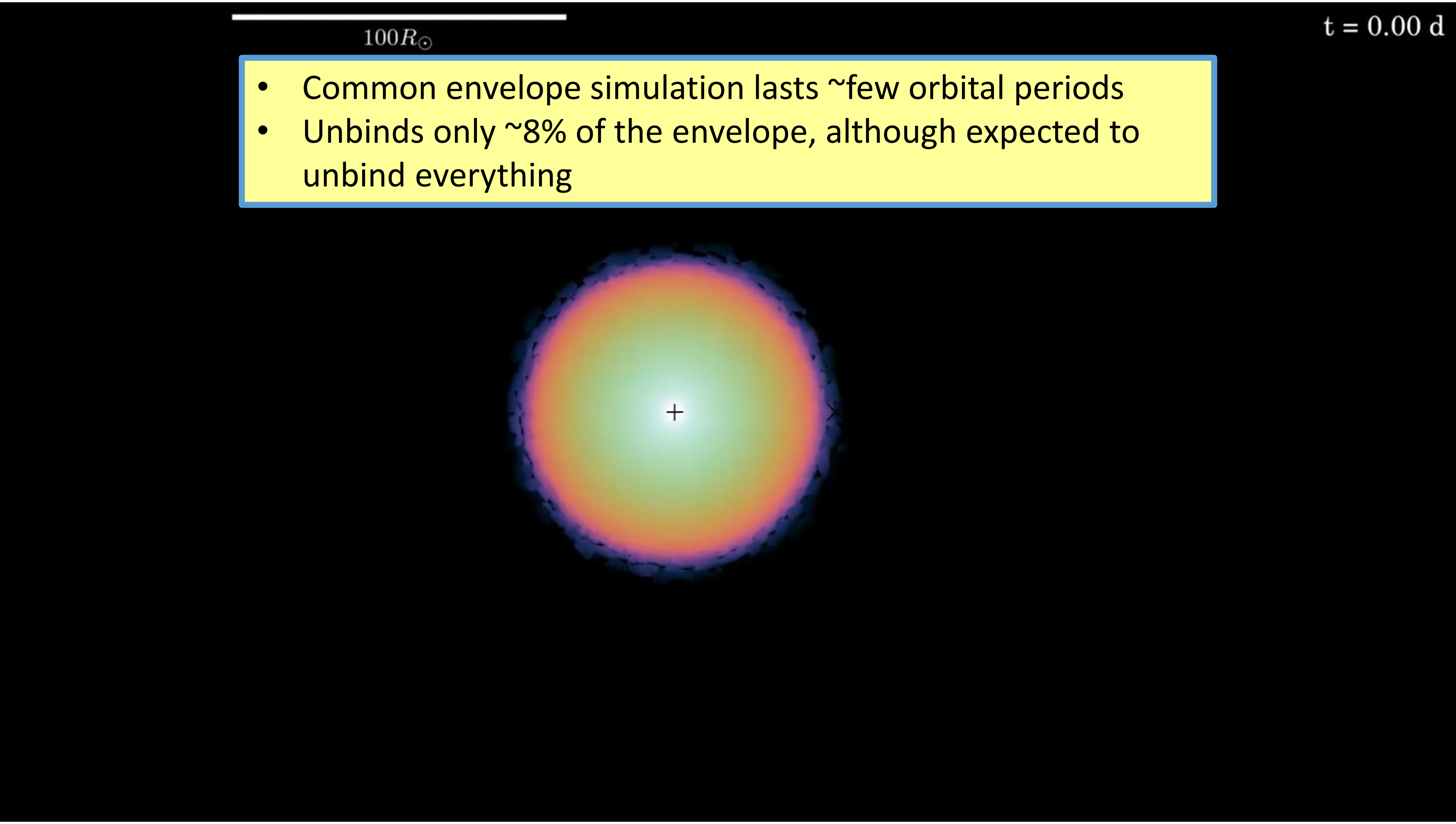

- Common envelope simulation lasts ~few orbital periods
- Unbinds only ~8% of the envelope, although expected to unbind everything

Ohlmann et al. (2016)

Predicting outcome of common envelope

$$E_{\rm bind} = \Delta E_{\rm orb} = E_{\rm orb,i} - E_{\rm orb,f} = -\frac{G m_1 m_2}{2a_{\rm i}} + \frac{G m_{1,\rm c} m_2}{2a_{\rm f}}$$

$$\frac{m_1 m_{1,\rm env}}{\lambda R_1} = \alpha_{\rm CE}\left(-\frac{G m_1 m_2}{2a_{\rm i}} + \frac{G m_{1,\rm c} m_2}{2a_{\rm f}}\right)$$

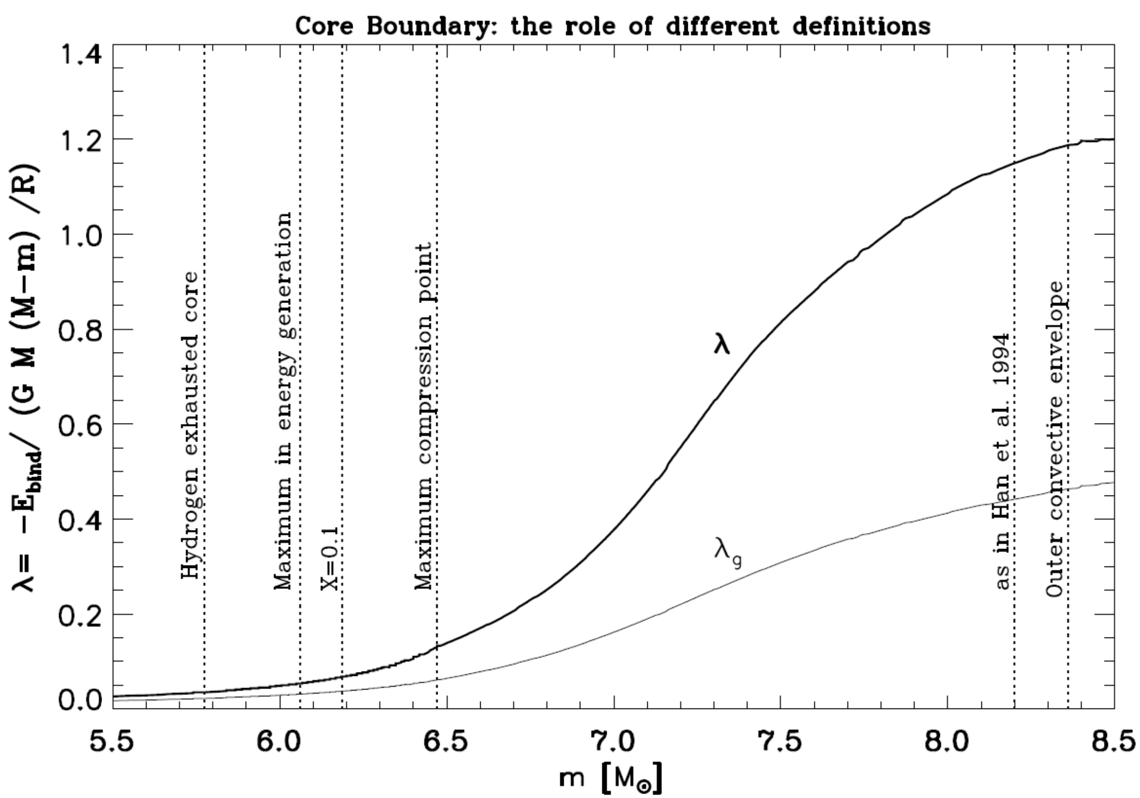

Ivanova et al. (2013)

Gravitational wave merger time

$$\tau_{merge}(a_o, e_o) \simeq \frac{768}{425}\tau_{circ}(a_o)(1 - e_o^2)^{7/2}$$

$$\tau_{circ}(a_o) = \frac{a_o^4}{4\beta}$$

$$\beta = \frac{64}{5}\frac{G^3}{c^5}m_1 m_2(m_1 + m_2)$$

Peters (1964)

Bringing stars in a binary together

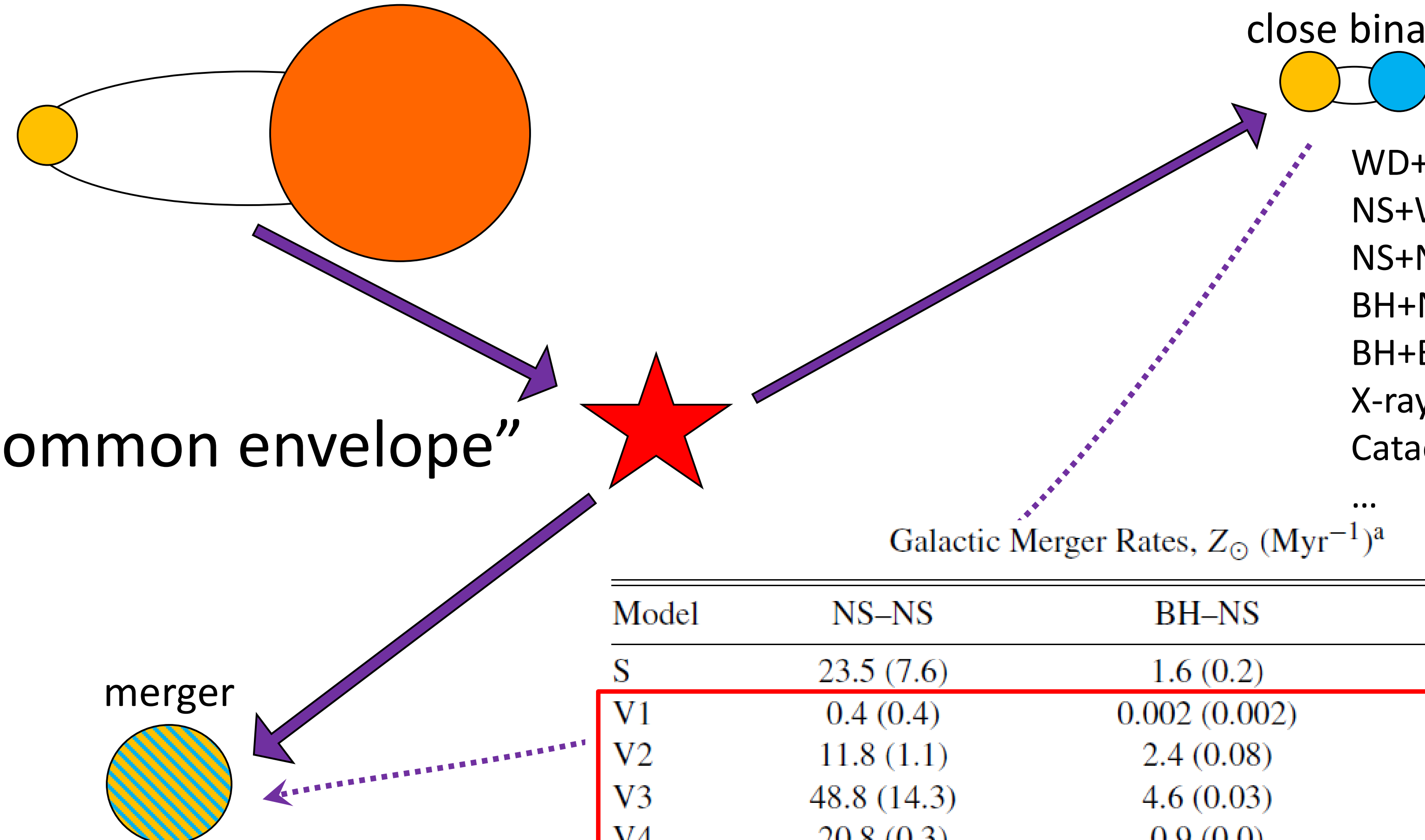

WD+WD
NS+WD
NS+NS
BH+NS
BH+BH
X-ray binaries
Cataclysmic variables
…

Galactic Merger Rates, $Z_{\odot}$ (Myr^{-1})[a]

Model	NS–NS	BH–NS	BH–BH
S	23.5 (7.6)	1.6 (0.2)	8.2 (1.9)
V1	0.4 (0.4)	0.002 (0.002)	1.1 (1.1)
V2	11.8 (1.1)	2.4 (0.08)	15.3 (0.4)
V3	48.8 (14.3)	4.6 (0.03)	5.0 (0.03)
V4	20.8 (0.3)	0.9 (0.0)	0.3 (0.0)

Dominik et al. (2012)

Blue stragglers
SN1987A progenitor
FK Com
η Car
…

SN Ia
short GRB/kilonovae
R CrB
…

Order-of-magnitude astrophysics

Does a 15 solar mass star release more energy during its stellar lifetime or when it explodes as a supernova? Which form of energy release is likely to have more impact on the surrounding interstellar medium?

Collapse of the core

Massive star death

1 erg = 10^{-7} J

1 $L_{\odot}$ = 3.9×10^{33} ergs/s

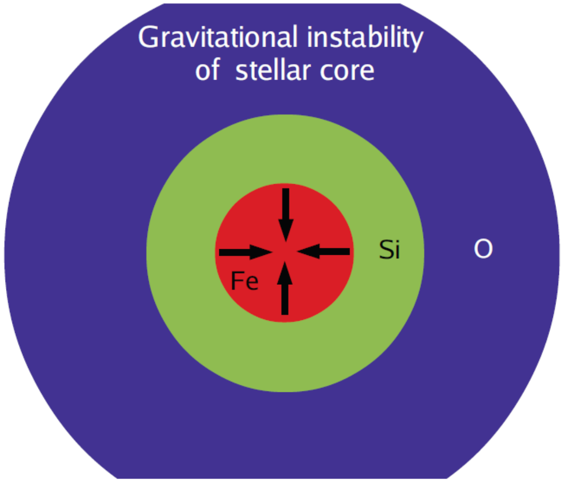

$M_{\mathrm{initial}} > 8\ M_{\odot}$
Collapse from WD size ~0.3s

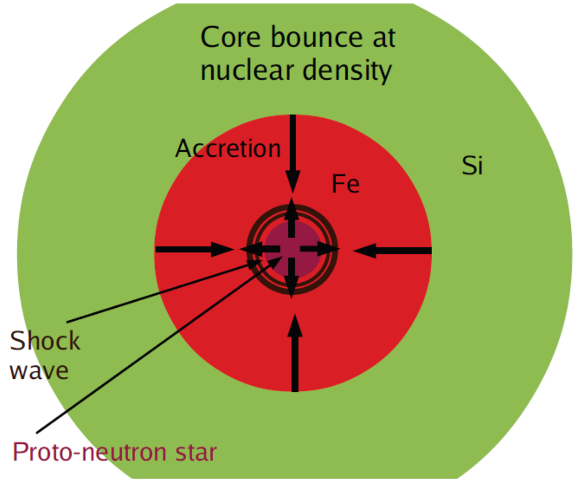

Proto-neutron star ~60 km
Binding energy ~ 3×10^{53} ergs

<10m s

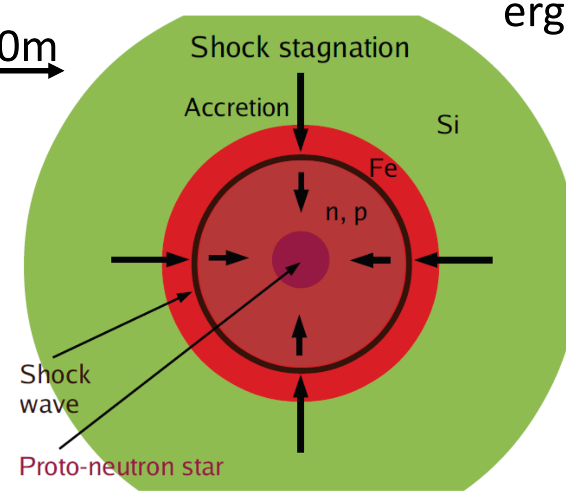

Stalled shock at 100-200 km
Neutrino cooling ~ 10^{52} ergs/s
Duration up to ~1 s

Reason not fully understood

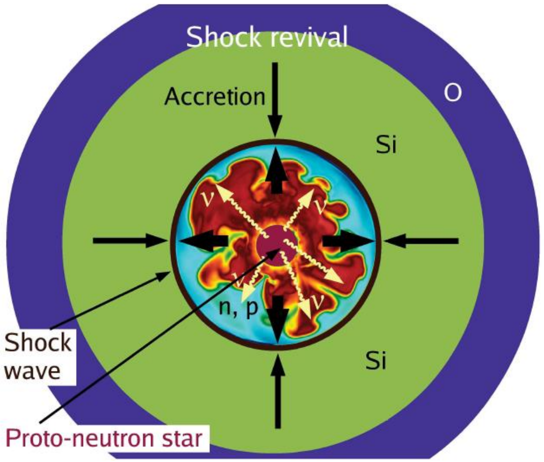

All NS binding energy released before 10-100s

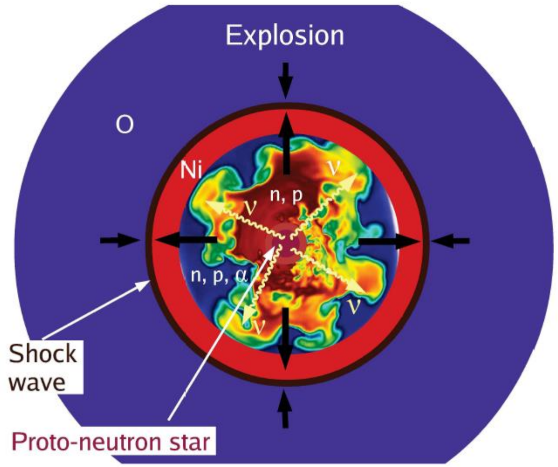

Explosion energy ~10^{51} ergs
$10^{-3} - 10^{-1}\ M_{\odot}$ of Nickel-56
Shock at surface in ~hours

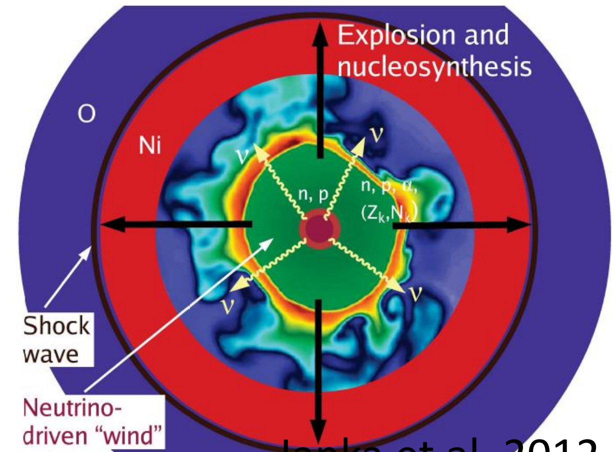

Janka et al. 2012

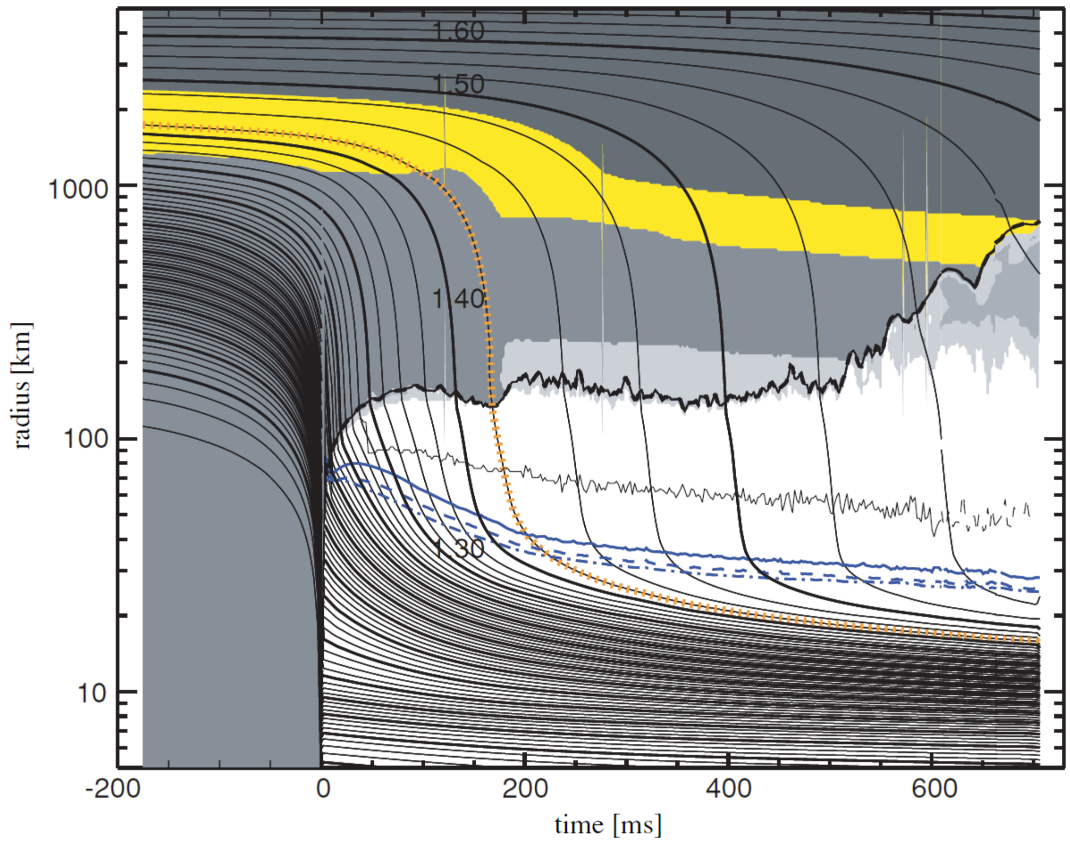

Figure 2. Time evolution of Model M15LS-rot visualized by the mass-shell trajectories. In this two-dimensional simulation with rotation, the mass-shell lines mark the radii of spheres that contain certain values of the rest mass (the plot is based on an evaluation of the mass-weighted lateral average of the two-dimensional data set). They are spaced in steps of 0.025 $M_\odot$ with bold lines every 0.1 $M_\odot$. The thick solid line starting at $t = 0$ denotes the mass-averaged shock position, the blue lines represent the mean neutrinospheres of ν_e (solid), $\bar{\nu}_e$ (dashed), and heavy-lepton neutrinos (dash-dotted), the black dashed curve shows the mean gain radius, and the location of the composition interface between the silicon shell and the oxygen-enriched Si layer of the progenitor star at 1.42 $M_\odot$ is highlighted by a red dashed line. Different shadings indicate regions with different chemical composition. Dark gray marks the layer where the mass fraction of oxygen is larger than 10% (which corresponds to the inner boundary of the layers that contain significant amounts of oxygen), medium gray the region where the mass fraction of heavy nuclei with mass numbers $A \geqslant 56$ exceeds 70%, the yellow band in between is the layer where both abundance constraints are not fulfilled (in this region silicon and sulfur are abundant), light gray indicates those regions where more than 30% of the mass is in α-particles, and the white areas enclosed by the shock front contain mostly free nucleons and only a small mass fraction (less than 30%) of α-particles. At times $t \gtrsim 600$ ms post bounce, slightly darker gray patches in the light-gray postshock regions contain a mass fraction of more than 60% helium nuclei. This signals that the nucleon recombination becomes more complete and/or that the dissociation of alpha particles to free nucleons is less complete in the matter expanding behind the outgoing shock because of low postshock temperatures when the shock reaches larger radii. Note that compressional heating triggers nuclear burning (described in our simulations by a "flashing treatment," see Section 2.1) and leads to changes of the chemical composition in the infalling stellar layers.

Marek & Janka (2009)

Problem with core-collapse supernovae

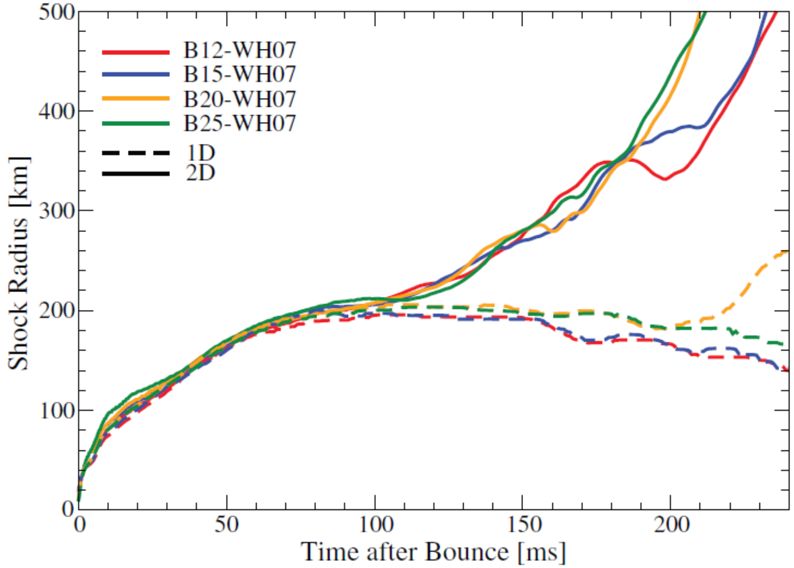

Bruenn et al. (2013)
4/4

Dolence et al. (2014) 0/4

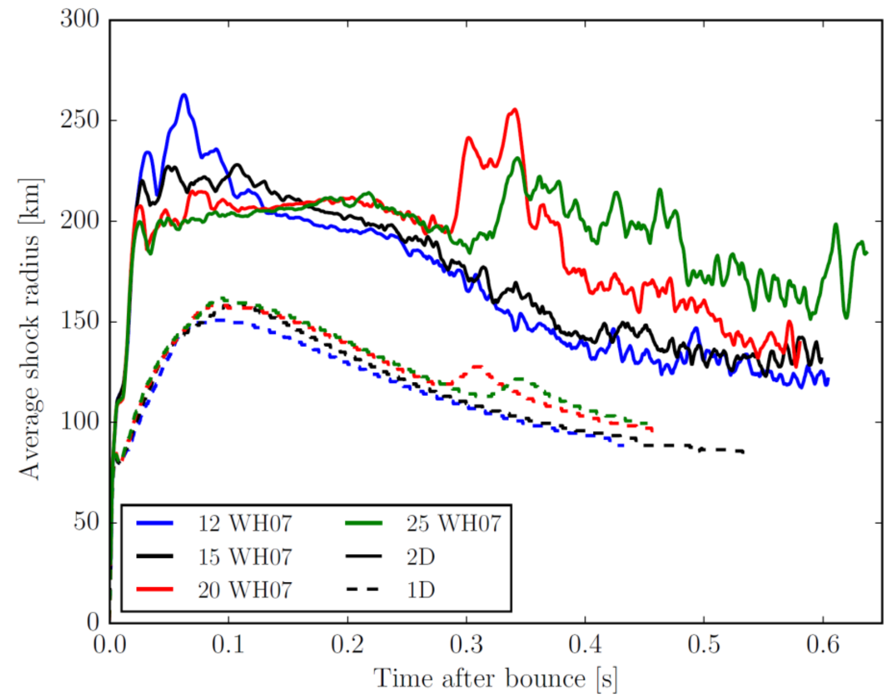

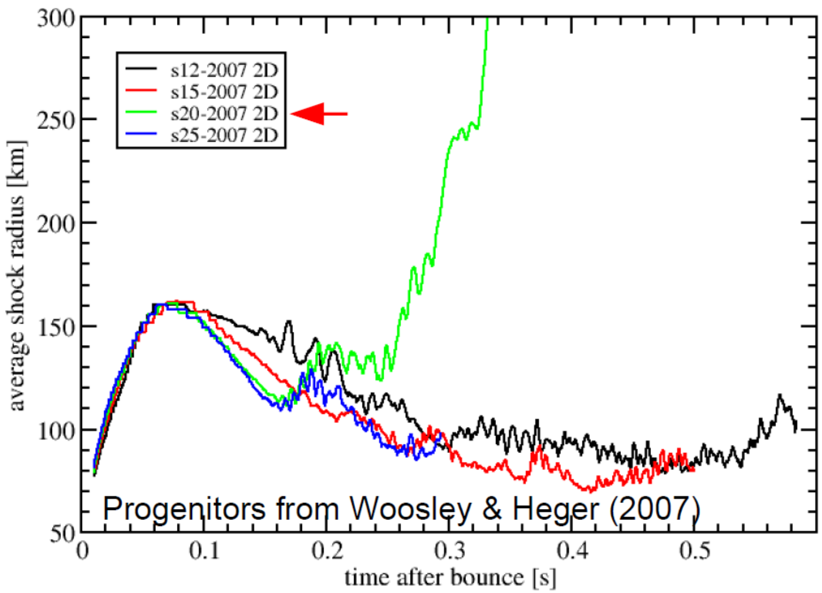

Muller et al. (2013) 1/4

Stalled accretion shock

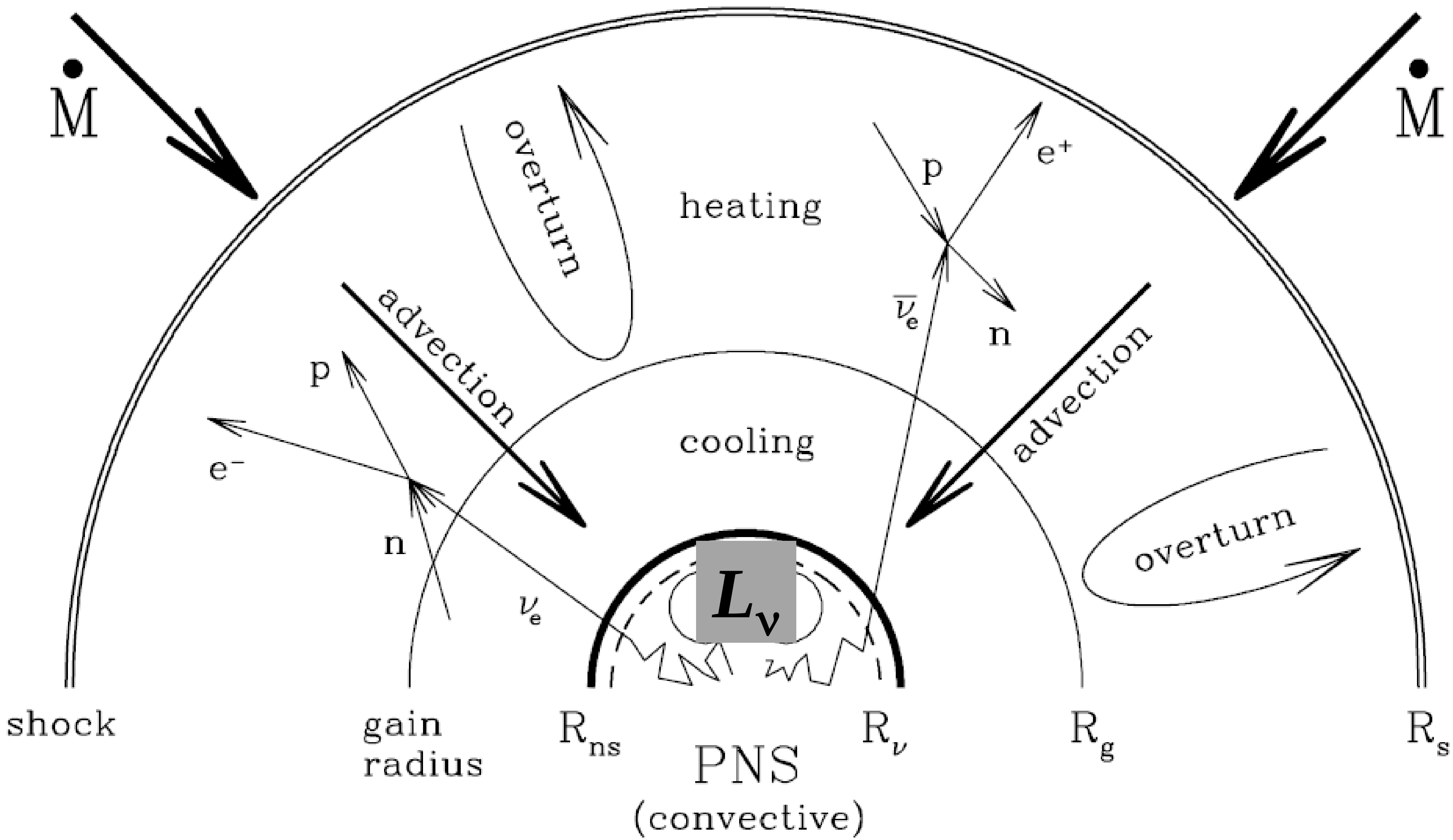

Janka (2001)

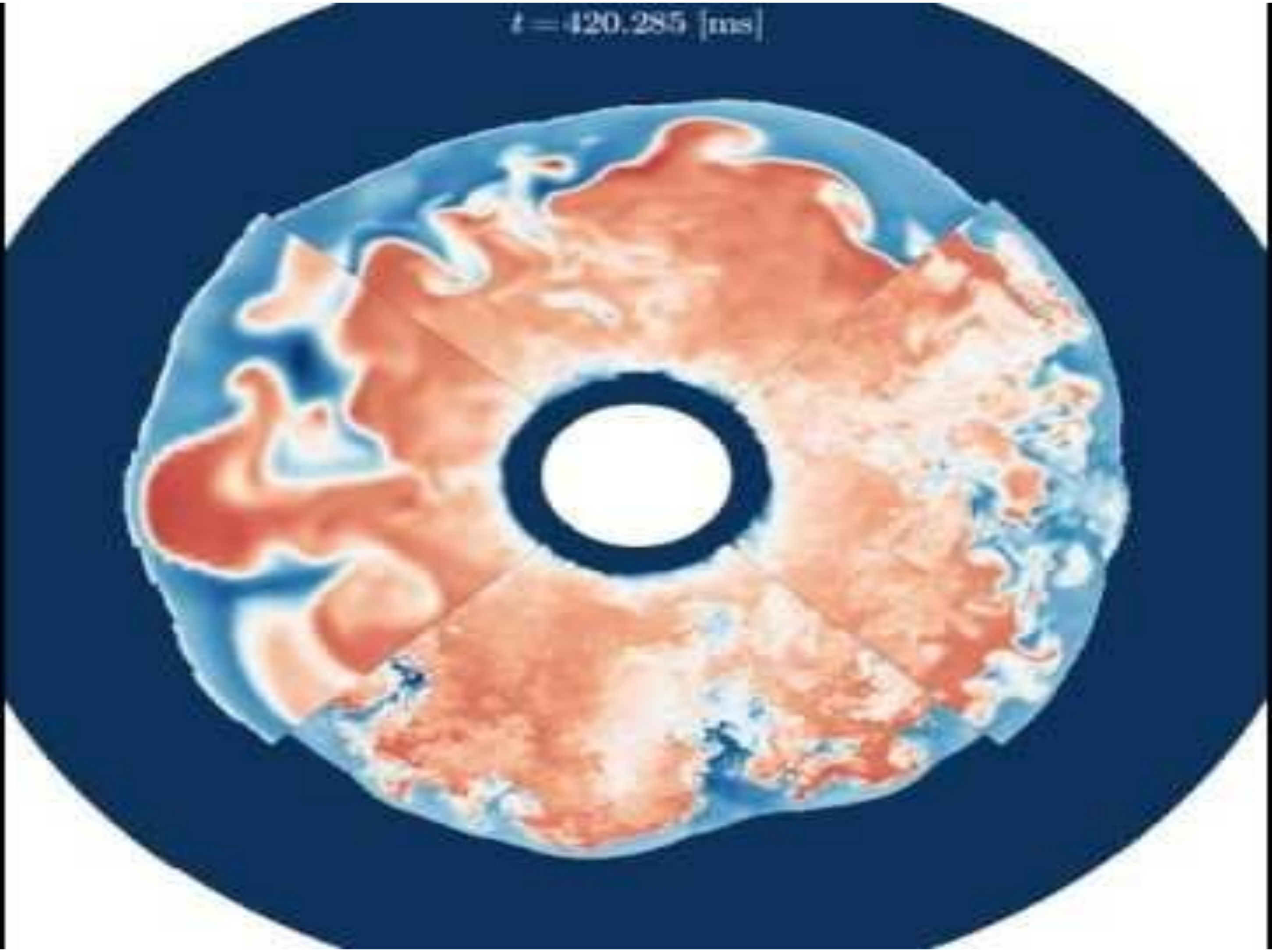

David Radice youtube

Neutrino reactions

Process
Beta-Processes
$\nu_e + n \rightleftharpoons e^- + p$
$\bar{\nu}_e + p \rightleftharpoons e^+ + n$
$\nu_e + (A,Z) \rightleftharpoons e^- + (A, Z+1)$
Scattering Reactions
$\nu + (A,Z) \rightleftharpoons \nu' + (A,Z)$
$\nu + N \rightleftharpoons \nu' + N$
$\nu + e^{\pm} \rightleftharpoons \nu' + e^{\pm}$
("Thermal") Pair Production
$\nu + \bar{\nu} \rightleftharpoons e^- + e^+$
Nucleon-Nucleon Bremsstrahlung
$\nu + \bar{\nu} + N + N \rightleftharpoons N + N$
Reactions between Neutrinos
$\nu_{\mu,\tau} + \bar{\nu}_{\mu,\tau} \rightleftharpoons \nu_e + \bar{\nu}_e$
$\nu_x + \{\nu_e, \bar{\nu}_e\} \rightleftharpoons \nu'_x + \{\nu'_e, \bar{\nu}'_e\}$

Janka (2012)

Collective neutrino oscillations

$$\mathsf{H} = \frac{\Delta m^2}{2E}\mathsf{B} + \lambda\mathsf{L} + \mathsf{H}_{\nu\nu} = \frac{\Delta m^2}{2E}\mathsf{B} + \sqrt{2}G_\mathrm{F} n_e \mathsf{L} + \sqrt{2}G_\mathrm{F}\int \mathrm{d}^3\mathbf{p}'(1 - \hat{\mathbf{p}}\cdot\hat{\mathbf{p}}')(\rho_{\mathbf{p}'} - \bar{\rho}_{\mathbf{p}'})$$

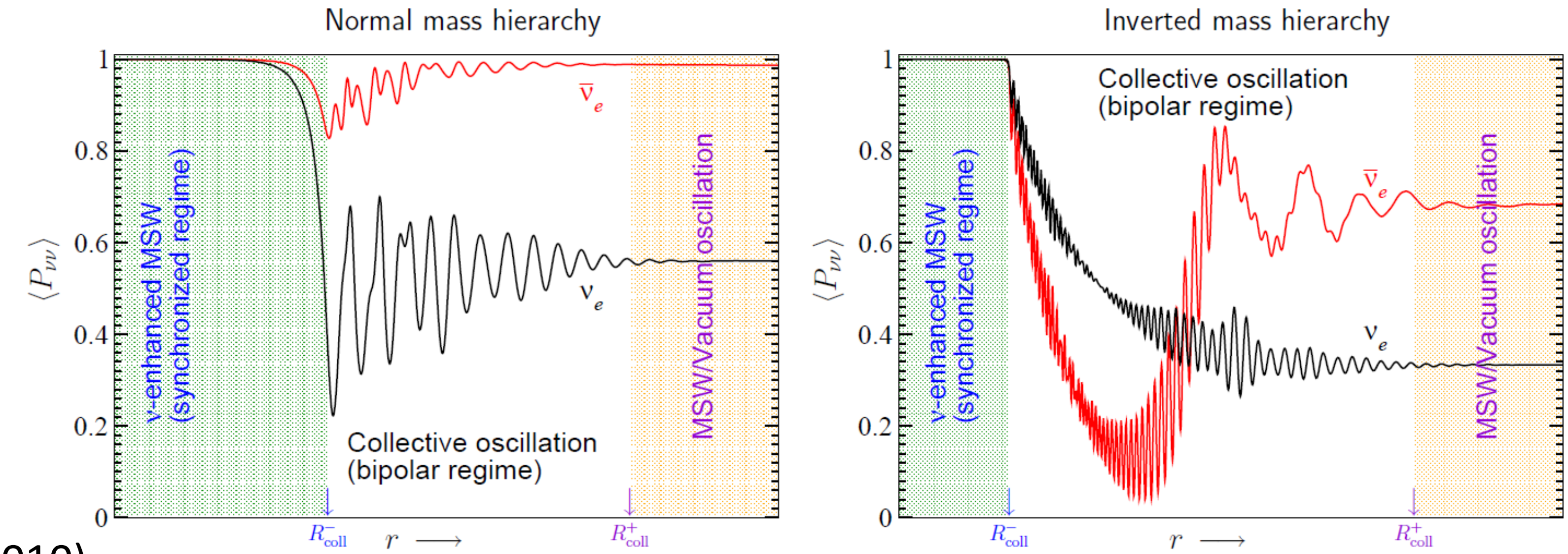

Duan et al. (2010)

How massive stars explode?

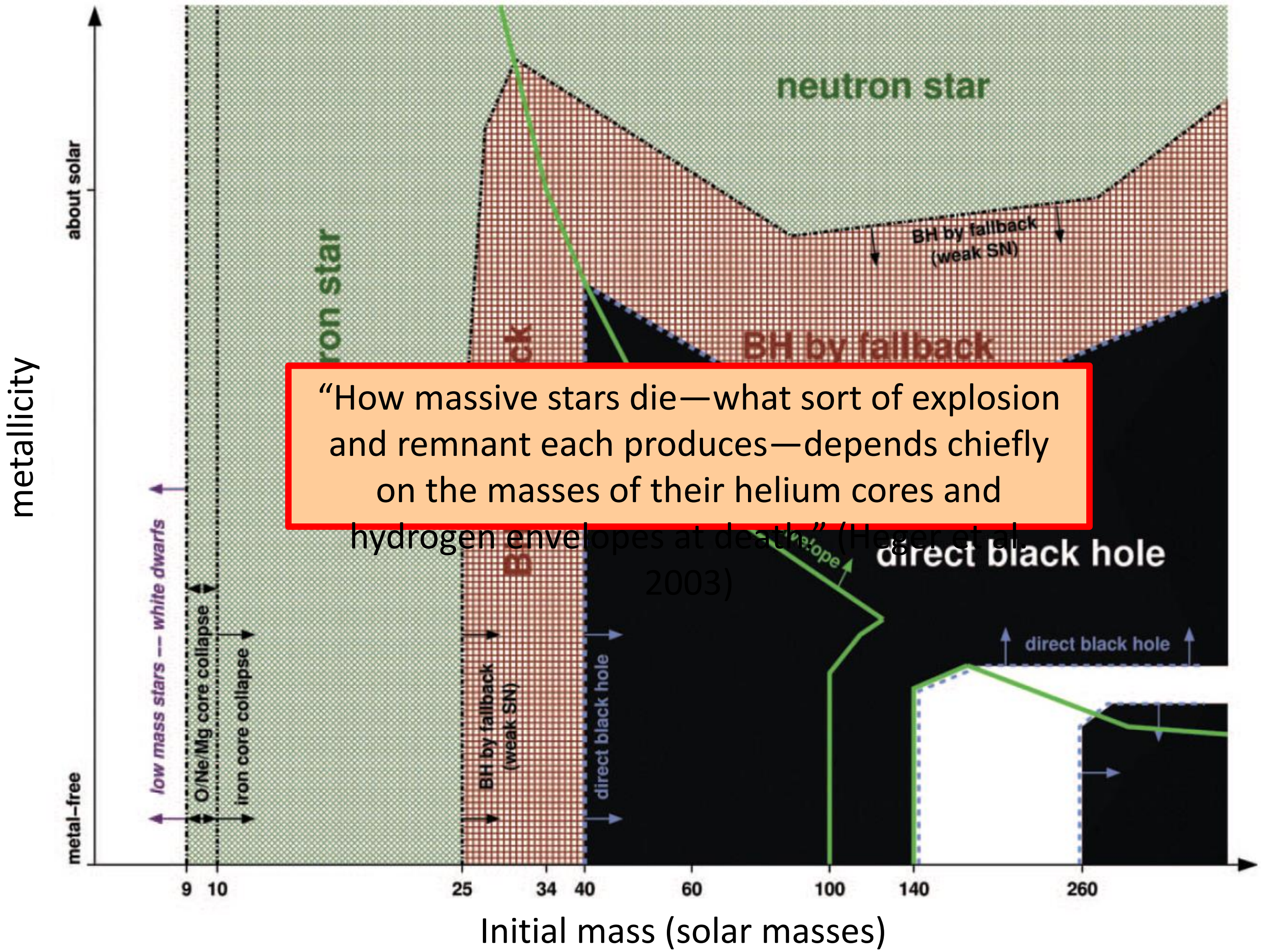

"How massive stars die—what sort of explosion and remnant each produces—depends chiefly on the masses of their helium cores and hydrogen envelopes at death" (Heger et al. 2003)

Heger et al. (2003)

Which stars explode?

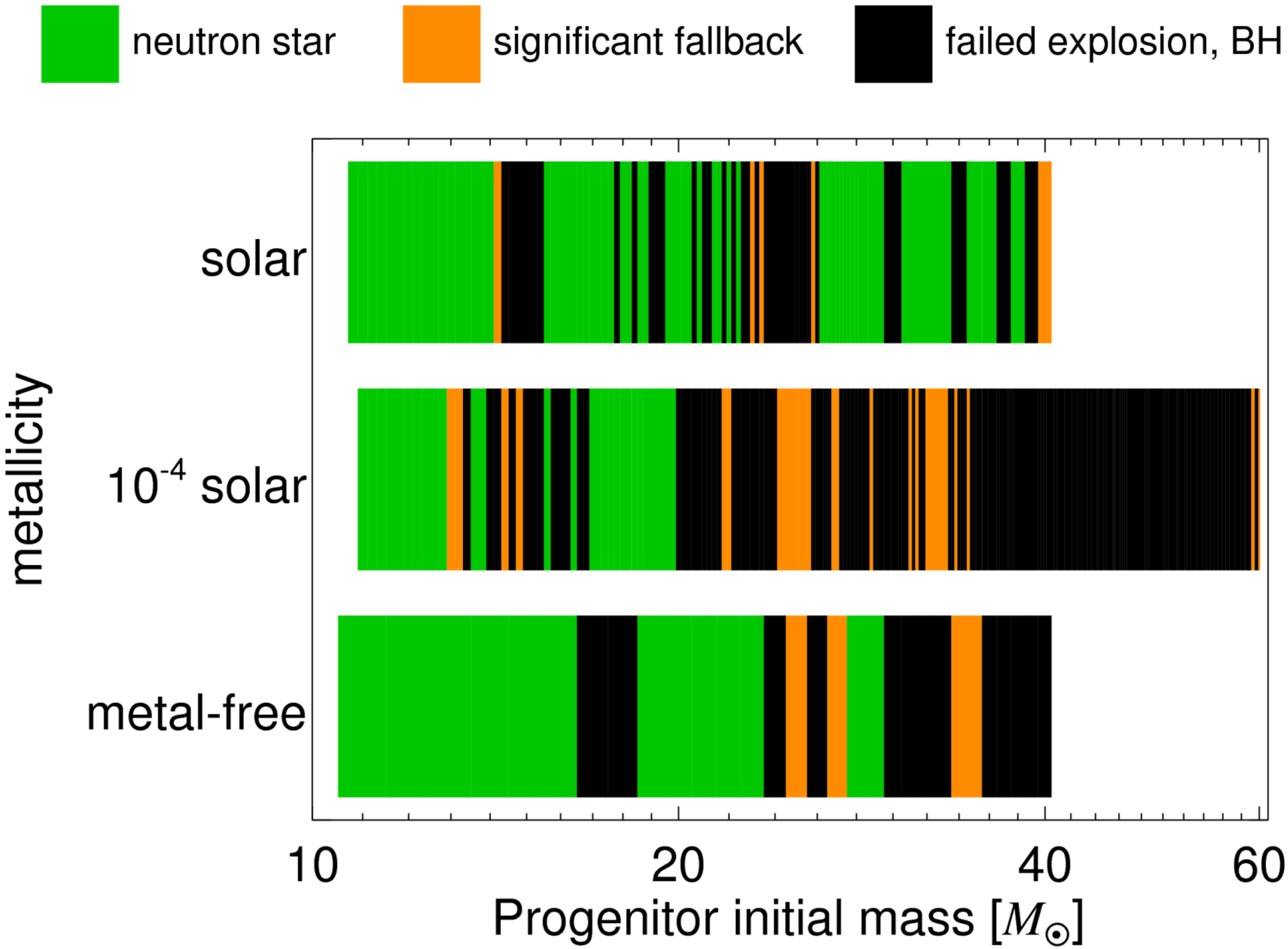

Pejcha & Thompson (2015)

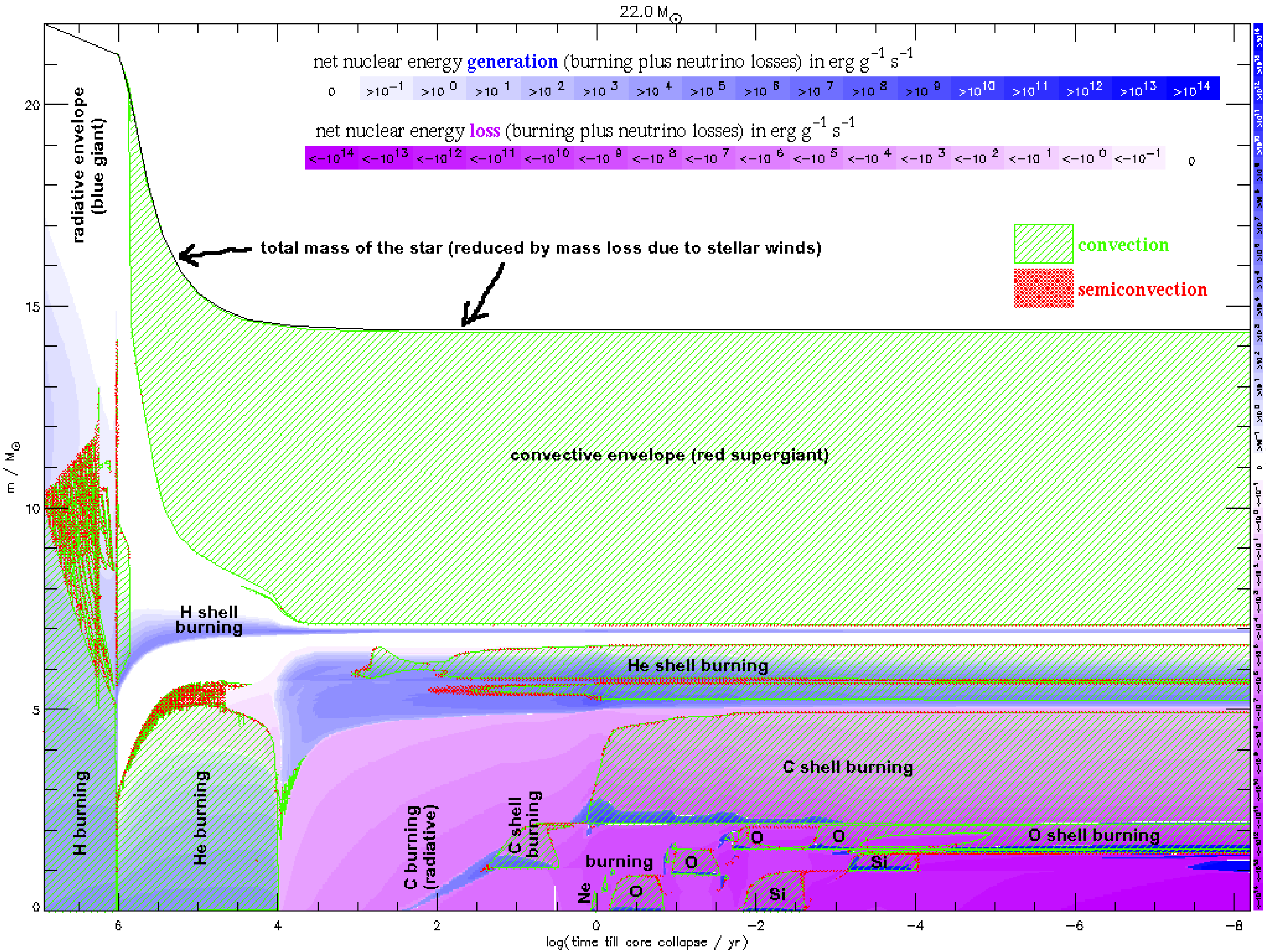

A. Heger website 2sn.org

Masses in the Stellar Graveyard

in Solar Masses

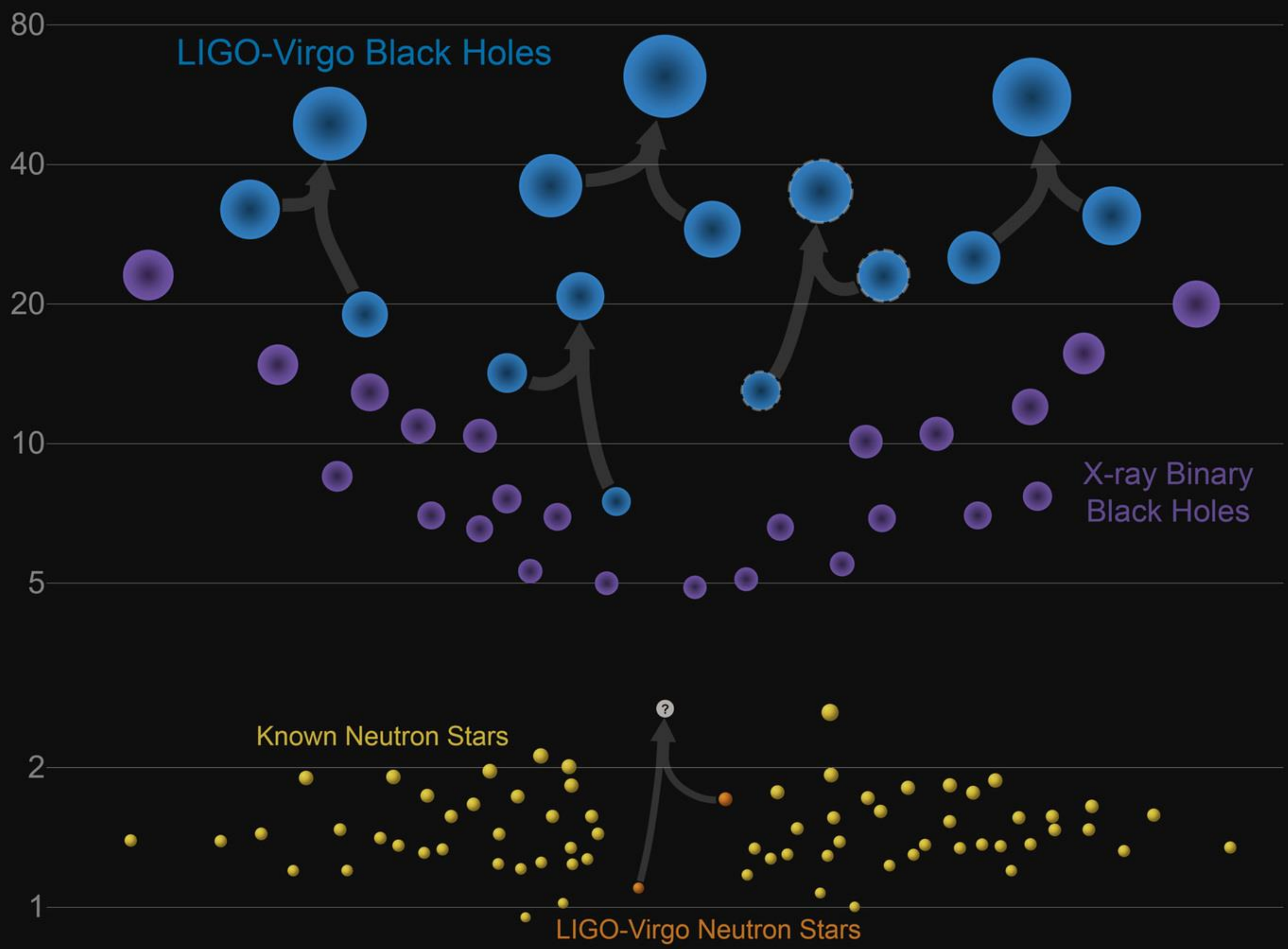

LIGO-Virgo/Frank Elavsky/Northwestern University